Remote Sensing of Environment 224 (2019) 289–303

Contents lists available at ScienceDirect

Remote Sensing of Environment

journal homepage: www.elsevier.com/locate/rse

Assessment and inter-comparison of recently developed/reprocessed microwave satellite soil moisture products using ISMN ground-based measurements

A. Al-Yaari[a,*], J.-P. Wigneron[a], W. Dorigo[b], A. Colliander[c], T. Pellarin[d], S. Hahn[b], A. Mialon[e], P. Richaume[e], R. Fernandez-Moran[f], L. Fan[a,g], Y.H. Kerr[e], G. De Lannoy[h]

[a] INRA, UMR1391 ISPA, Villenave d'Ornon, France
[b] Department of Geodesy and Geoinformation, Vienna University of Technology, Vienna, Austria
[c] NASA Jet Propulsion Laboratory, California Institute of Technology, Pasadena, CA 91109, USA
[d] Univ. Grenoble Alpes, CNRS, IRD, Grenoble INP, IGE, F-38000 Grenoble, France
[e] Université de Toulouse, CNES, CNRS,INRA, IRD, UPS, UMR 5126, Toulouse, France
[f] University of Valencia, IPL (Image Processing Laboratory), Spain
[g] Collaborative Innovation Center on Forecast and Evaluation of Meteorological Disaster, School of Geographical Sciences, Nanjing University of Information Science and Technology, Nanjing 210044, China
[h] KU Leuven, Department of Earth and Environmental Sciences, 3001 Heverlee, Belgium

ARTICLE INFO

Keywords:
Soil moisture
International soil moisture network
Passive microwave remote sensing
Active microwave remote sensing
Evaluation
Review

ABSTRACT

Soil moisture (SM) is a key state variable in understanding the climate system through its control on the land surface energy, water budget partitioning, and the carbon cycle. Monitoring SM at regional scale has become possible thanks to microwave remote sensing. In the past two decades, several satellites were launched carrying on board either radiometer (passive) or radar (active) or both sensors in different frequency bands with various spatial and temporal resolutions. Soil moisture algorithms are in rapid development and their improvements/revisions are ongoing. The latest SM retrieval products and versions of products that have been recently released are not yet, to our knowledge, comprehensively evaluated and inter-compared over different ecoregions and climate conditions. The aim of this paper is to comprehensively evaluate the most recent microwave-based SM retrieval products available from NASA's (National Aeronautics and Space Administration) SMAP (Soil Moisture Active Passive) satellite, ESA's led mission (European Space Agency) SMOS (Soil Moisture and Ocean Salinity) satellite, ASCAT (Advanced Scatterometer) sensor on board the meteorological operational (Metop) platforms Metop-A and Metop-B, and the ESA Climate Change Initiative (CCI) blended long-term SM time series. More specifically, in this study we compared SMAPL3 V4, SMOSL3 V300, SMOSL2 V650, ASCAT H111, and CCI V04.2 and the new SMOS-IC (V105) SM product. This evaluation was achieved using four statistical scores: Pearson correlation (considering both original observations and anomalies), RMSE, unbiased RMSE, and Bias between remotely-sensed SM retrievals and ground-based measurements from > 1000 stations from 17 monitoring networks, spread over the globe, disseminated through the International Soil Moisture Network (ISMN). The analysis reveals that the performance of the remotely-sensed SM retrievals generally varies depending on ecoregions, land cover types, climate conditions, and between the monitoring networks. It also reveals that temporal sampling of the data, the frequency of data in time and the spatial coverage, affect the performance metrics. Overall, the performance of SMAP and SMOS-IC products compared slightly better with respect to the ISMN in situ observations than the other remotely-sensed products.

1. Introduction

Surface soil moisture (i.e. the water content in the first few centimeters of the soil; referred to as SM in the following) is a key state variable in better understanding the climate system through controlling land surface energy, water budget partitioning (Chen et al., 2016; Koster et al., 2004; Miralles et al., 2014a; Miralles et al., 2014b; Pitman, 2003; Seneviratne et al., 2010; Seneviratne et al., 2013), and its

* Corresponding author.
E-mail address: amen.al-yaari@inra.fr (A. Al-Yaari).

https://doi.org/10.1016/j.rse.2019.02.008
Received 22 November 2018; Received in revised form 4 February 2019; Accepted 9 February 2019
Available online 21 February 2019
0034-4257/ © 2019 Elsevier Inc. All rights reserved.

important role in the carbon cycle (Jung et al., 2017). Monitoring SM at the regional scale has become possible thanks to active and passive microwave remote sensing. In the past two decades, several satellites were launched carrying either a radiometer (passive) or radar (active) or both, using frequency bands with various spatial and temporal resolutions. These satellites (or sensors) include, but are not limited to, SMAP (Soil Moisture Active Passive) launched by the National Aeronautics and Space Administration (NASA) in 2015 (Entekhabi et al., 2010), SMOS (Soil Moisture and Ocean Salinity) launched by the European space agency (ESA) in 2009 (Kerr et al., 2001), and ASCAT (Advanced Scatterometer) (Wagner et al., 2013) on board the meteorological operational (Metop) platforms Metop-A, Metop-B, and Metop-C. Since then, SM was retrieved from either brightness temperature (passive) or backscatter coefficient (active) observations relying mainly on radiative transfer model inversion (passive; Mo et al., 1982), change detection (active; Wagner et al., 1999), or neural network algorithms (Kolassa et al., 2018; Rodríguez-Fernández et al., 2016). These remotely sensed SM products are provided separately or blended (such as the one produced by the ESA project: Climate Change Initiative (CCI) SM long time series (Dorigo et al., 2017; Liu et al., 2012)).

Performance evaluation of these remotely-sensed SM retrievals is important to help improving satellite products and evaluating their interest for possible applications in climate, hydrology, and natural hazards (flood, drought, etc.). Numerous validation/evaluation studies of satellite-based SM retrievals have been conducted during the last decade (e.g., Al-Yaari et al., 2014a; Al-Yaari et al., 2014b; Al-Yaari et al., 2015; Al-Yaari et al., 2017; Albergel et al., 2009; Albergel et al., 2012; Brocca et al., 2011; Colliander et al., 2017; Dorigo et al., 2015; Draper et al., 2009; Kerr et al., 2016; Pierdicca et al., 2013; Sahoo et al., 2008; Su et al., 2013) using different approaches (e.g., sparse and dense networks, core validation sites, field campaigns, inter-comparisons among satellites, model simulations, etc.). However, SM retrieval algorithms are in rapid development and their improvements/revisions are ongoing adopting new concepts or conducting new calibrations; thus improving parameterizations and optimizing parameters in the algorithms (Wigneron et al., 2017). Therefore, new SM products and new versions of SM products have been released that are not, to our knowledge, comprehensively evaluated and inter-compared yet. One such new product is the SMOS-IC SM product, which was recently developed by INRA (Institut National de la Recherche Agronomique) in collaboration with CESBIO (Centre d'Etudes Spatiales de la BIOsphere) (Fernandez-Moran et al., 2017b). To our knowledge, the last SMOS-IC version has only been evaluated against modelled SM data from ECMWF (Fernandez-Moran et al., 2017b), although a previous version was already tested using several in situ datasets from ISMN (International Soil Moisture Network) for the period 2011–2013 (Fernandez-Moran et al., 2017a). The objective of this study is to evaluate the SMOS-IC SM product along with the most recent versions, available at the time of writing, of five other satellite-based SM products, namely: NASA SMAP Level 3 (V4), ESA SMOS Level 3 (V300) and Level 2 (V650), ASCAT (H111), and the CCI long-term record SM (V04.2). This was achieved using ground-based surface SM measurements from the ISMN (Dorigo et al., 2011; Dorigo et al., 2013). For the passive sensors, we limited this study to L-band SM retrievals which are more optimal for monitoring SM. Other key SM observations (AMSR-E/AMSR2) were merged in the CCI product. This paper is organized as follows. The datasets and scores used are briefly described in Section 2. Results and discussion are presented in Sections 3 and 4, respectively. Finally, concluding remarks are given in Section 5.

2. Materials and methods

2.1. Datasets

Table 1 presents an overview of the SM products used in this study. More details are given in the following subsections.

2.1.1. SMOS

The SMOS satellite, developed by ESA with contributions from CNES (Centre National d'Etudes Spatiales) and CDTI (Centro para el Desarrollo Tecnológico Industrial), is the first polar orbiting L-Band (1.4 GHz) radiometer, with a spatial resolution of (~43 km) and 3-day revisit. The SMOS satellite mission has been providing fully polarized brightness temperature (TB, level 1) observations since 2010 and over a range of incidence angles (~0–60°) (Kerr et al., 2010). These SMOS TB observations are used to retrieve SM and vegetation optical depth (VOD) using a forward emission model, namely, the L-band Microwave Emission of the Biosphere (L-MEB) model (Wigneron et al., 2007). The retrieval approach is simply based on iterative estimation of SM and VOD values providing the lowest difference between modelled and observed TB data by minimizing a cost function (sum of the squared weighted differences between modelled and observed TB) (Wigneron et al., 2000).

Currently, there are three main physically-based SMOS SM retrieval products available (SMOS-IC, SMOS Level 2 (L2), and SMOS Level 3 (L3)), for which all: (i) use the L-MEB radiative transfer model (ii) provide SM as volumetric water content (m^3/m^3) with global coverage of 3 days; (iv) provide data at both ascending (06:00 am) and descending (06:00 pm) orbits; (vi) adopt the NETCDF format for the products; and (vii) use the European Centre for Medium-Range Weather Forecasts (ECMWF) soil temperature products. However, the products differ by the projection and grid used as well as with the temporal aggregation for L3 products sampling, as detailed below. It should be noted that SMOS provides also root zone SM at 0–1 m known as Level 4.

2.1.1.1. SMOS-IC. In this study, we used the SMOS-IC V105 SM product. The SMOS-IC SM product is based on a relatively simple approach that considers homogeneous pixels (unlike SMOSL3 and SMOSL2 where the details of the SMOS footprint at a resolution of 4 km × 4 km are taken into account), to avoid possible uncertainties and errors associated with the datasets used to characterize the heterogeneity of the pixel in the SMOSL2 and SMOSL3 algorithms. The SMOS-IC inversion algorithm aims at a minimal use of auxiliary data through the optimal use of the multi-angular TB observations. Therefore, SMOS-IC (unlike SMOSL2 and SMOSL3) does not use ECMWF SM or the Moderate Resolution Imaging Spectroradiometer (MODIS) LAI (Leaf Area Index) products as first guesses and in the simulation of TB over heterogeneous pixels including forested areas. In SMOS-IC, the effective vegetation scattering albedo (ω) parameter was optimized using the ISMN in-situ observations (Fernandez-Moran et al., 2017a) and the roughness parameters were derived from the global map of Parrens et al. (2016). The "optimization" process of ω led to a very simple result: $\omega \sim 0.1$ over low vegetation and bare soils, while $\omega \sim 0.06$ over forested areas. Also, SMOS-IC does not take into account the corrections associated with the characterization of the antenna patterns as a function of viewing angle and azimuth. To filter out observations/retrievals strongly impacted by RFI (Radio Frequency Interferences) effects, SMOS-IC SM retrievals were excluded when the Root Mean Square Error (RMSE) between SMOSL3 TB and simulated TB > 10 K in the present study. SMOS-IC is currently delivered as a scientific product in the Equal-Area Scalable Earth (EASE) grid version 2 at 25 km resolution and publicly available at CATDS (Centre Aval de Traitement des Données SMOS):

https://www.catds.fr/Products/Available-products-from-CEC-SM/SMOS-IC. Note that although SMOS-IC was recently released, it corresponds to the initial SMOS 2-Parameter retrieval approach, relying on the relatively low temporal variation of VOD, and fully described in Wigneron et al. (2000). Also note that SMOS-IC is currently in its first version and is thus prone to evolve and progress as it is still undergoing refinements and improvements.

2.1.1.2. SMOSL2. In this study, we used the SMOSL2 SM product in version V650. There are some changes in this version relative to the

Table 1
Overview of all soil moisture data sets under investigation.

	Passive		Active	Combined (CCI)
Sensor	SMOS	SMAP	ASCAT	SMMR SSM/I TMI AMSRE AMSR2 Windsat ERS ASCAT SMOS
Satellite	SMOS	SMAP	Metop-A & Metop-B	Various
Time period	Jan 2010–present	Mar 2015–present	Jan 2007–present	Jan 1978–Dec 2016
Band frequency	1.4 GHz	1.4 GHz	5.3 GHz	1.4–19.3 GHz
Spatial sampling	15 km DGG - 25 km EASEv2	36 km EASEv2	12.5 km	0.25°
Sensor resolution	27–55 km	43 km	25–34 km	various
Spatial coverage	Global	Global	Global	Global
Acquisition time	Descending: 06:00 pm Ascending: 06:00 am	Descending: 06:00 am Ascending: 06:00 pm	Descending: 09:30 am Ascending 9:30 pm	–
Product version	SMOSL2 V650 SMOSL3 V300 SMOS-IC V105	SMAPL3 V4	H111	CCI V04.2
Unit	m^3/m^3	m^3/m^3	Degree of saturation (%)	m^3/m^3

previous ones (e.g., V620) such as updating some processing parameters (e.g., Chi^2 rescaling), configuration (that can be used for additional quality control checks), and auxiliary files. The most important one is replacing the ECOCLIMAP (218 ecosystems) database (Masson et al., 2003) with the International Geosphere Biosphere Programme (IGBP; 17 land cover classes) land cover map (Friedl et al., 2010), which is also used by the SMAP Level 2 algorithm. This change influences the distribution of the forested areas (FO) and the nominal vegetated soil and therefore leads to different SM values from previous versions.

SMOSL2 (and SMOSL3) algorithm considers pixel heterogeneity and inversion is done on the dominant fraction: low vegetation, bare soil or forest and water surfaces. On the non-dominant fraction, auxiliary information (e.g., ECMWF SM and MODIS LAI_{Fmax}, the maximum yearly value of LAI) is used to simulate TB and to better constrain the model inversion. However, these auxiliary data contain errors that can propagate in the inversion algorithm, which may lead to noise and bias in the SM retrievals. In the latest SMOSL2 version, ECMWF SM is used to simulate TB over heterogeneous pixels including forested areas after rescaling. This was done by using cumulative distribution function (CDF) matching, to better match to the histogram of the SMOS SM retrieved values.

SMOSL2 SM is provided in swath mode in the Icosahedral Equal Area (ISEA) 4H9 Discrete Global Grid (DGG) at 15 km resolution and can be freely obtained from the ESA website portal https://earth.esa.int/web/guest/missions/esa-operational-eo-missions/smos. Readers are referred to Kerr et al. (2012) for more details. SMOSL2 SM retrievals were filtered excluding the following: Chi^2 index (i.e. retrieval fit quality index between the observed SMOS TBs and the simulated TBs) > 3 and RFI > 20%; where RFI was calculated as follows:

$$RFI = \frac{NRFI_x + NRFI_y}{MAVA0} \quad (1)$$

where:

NRFIx: is the number of TB flagged for RFI in the X–direction.
NRFIy: is the number of TB flagged for RFI in the Y–direction.
MAVA0: is the total number of TB observations at this point.

2.1.1.3. SMOSL3. The SMOSL3 SM algorithm is based on the same complex approach (i.e. accounting for heterogeneity) used in the SMOSL2 but enhanced through a multi-orbit algorithm that uses retrievals from several revisits over a seven day window (Al Bitar et al., 2017; Jacquette et al., 2013). In addition, the objective of SMOSL3 is to provide enhanced products that are easier to process by the scientific community, given as daily, aggregated in 3-days (moving window mean), 10-days (median, minimum and maximum values), and monthly (mean) global maps. Here we used the daily SMOSL3 version 300, which can be freely obtained from the CATDS website portal in the EASE grid v2 (25 km), which is much easier to process than the grid used in the SMOSL2 processor. SMOSL3 SM retrievals were excluded when RFI > 20%. Readers are referred to Al Bitar et al. (2017) for more details about SMOSL3.

It should be noted here that the soil roughness and effective vegetation scattering albedo parameters used in SMOSL2 and SMOSL3 are still pre-launch values and thus different from those currently used in the SMOS-IC algorithm. Also note that SMOSL3 is based upon an older version of L2 and that a bug was identified in the current SMOSL3 algorithm (V300) and will be corrected in the next version.

2.1.2. SMAP

SMAP is a NASA satellite mission that was launched in 2015 to monitor global SM and landscape freeze/thaw state (Entekhabi et al., 2010). The SMAP satellite carries a radiometer (operational; 1.41 GHz) and radar (stopped working after about three months of operation; 1.26 GHz) operating in the L-band frequency. The spatial resolution of radar and radiometer is ~3 km and ~40 km, respectively, with a 1000-km swath width and a constant 40-degree incidence angle. The SMAP mission provides surface (~5 cm) SM (Chan et al., 2016) and root zone SM (1 m; Reichle et al., 2017); and also other geophysical variables such as landscape freeze/thaw (Derksen et al., 2017) and net ecosystem exchange of carbon (NEE) (Jones et al., 2017). Like SMOS, different levels of SM products are delivered as half-orbit products (swath based product; SMAPL2), daily gridded composites (SMAPL3), and model-assimilated products i.e. SMAPL4. In this study, we used the 36-km EASEv2 gridded L3SMP. V4 SM product (only when the retrieval quality is recommended i.e. unfrozen soils and a vegetation water content < 5 kg/m^2). This version (herein referred to as SMAP) was preceded by a beta quality version (released in 2015) and Version 3 validated SM data (released in 2016) (O'Neill et al., 2017).

2.1.3. ASCAT

The Advanced Scatterometer (ASCAT) is a real aperture radar carried on-board Metop-A satellite that was launched in October 2006, followed by Metop-B satellite launched in September 2012 (PUM,

2016). Both satellites share the same sun-synchronous near-polar orbit and are half an orbital period apart from each other (~50 min.). The mean local solar time of the descending node is 9:30 a.m. and 9:30 p.m. for the ascending node. ASCAT operates in the C-band frequency (VV polarization) and measures the Normalized Radar Cross Section (NRCS), also known as backscatter coefficient. The two main ASCAT level 1b backscatter products are provided at a spatial resolution of 25–34 km and 50 km. The Vienna University of Technology (TU Wien) semi-empirical change detection algorithm exploits the multi-angle backscatter measurements from ASCAT in order to obtain surface SM expressed in degree of saturation (Wagner et al., 1999).

In this study, we used Metop ASCAT Surface SM Climate Data Record (CDR) time series obtained from the Satellite Application Facility on Support to Operational Hydrology and Water Management (H SAF), namely, H111 - Metop ASCAT SSM CDR2016: Metop ASCAT SM CDR2016 time series with 12.5 km spatial sampling. Soil moisture values were only kept when the confidence flag [frozen or snow cover probability > 50% and using the Surface State Flag (SSF) information] = 0 (Paulik et al., 2014). The relative surface SM given in degree of saturation was converted into absolute SM (expressed in m^3/m^3) using porosity information (provided with the ASCAT datasets) computed from the Harmonized World Soil Database (HWSD (FAO et al., 2012)) using the formulas of Saxton and Rawls (2006). It should be noted that, root zone SM index is produced based on ASCAT SM assimilation in the ECMWF Land Data Assimilation System, namely the H-SAF SM-DAS-2 product. The reader is referred to the Product User Manual (PUM) for more details (PUM, 2016) about ASCAT SM.

2.1.4. ESA CCI soil moisture

The ESA CCI combined SM product is produced by merging both passive and active SM products (Liu et al., 2012) and available over 11/1978–12/2016 on global scale. These include scatterometer-based SM data (ERS ½, Metop A/B ASCAT) and radiometer-based SM data (SMMR, SSM/I, TMI, AMSR-E, WindSat, AMSR2, and SMOS). The merging between active and passive SM products is done based on a weighted average method with the weights being proportional to Signal to Noise Ratio (SNR; estimated using triple collocation analysis) of each product (Dorigo et al., 2017; Gruber et al., 2017). It should be noted that all these different datasets are scaled to a common model SM climatology, provided by the Global Land Data Assimilation System (GLDAS) Noah Land Surface Model (Rodell et al., 2004) using a CDF matching technique. Therefore, this study will show the Bias values but will not discuss them as they reflect the GLDAS model.

Regions of frozen soils or snow covered soils were already masked in the product obtained from the level 2 quality flags and no data are provided over rainforest regions (Dorigo et al., 2017). More details about the theoretical and algorithmic base of this product and detailed analysis about the uncertainties of the SM datasets can be found in (Dorigo et al., 2017; Gruber et al., 2017; Liu et al., 2012). The reader is also referred to http://www.esa-soilmoisture-cci.org for more information about the daily CCI volumetric (m^3/m^3) SM product, which is provided in a NETCDF format with a spatial resolution of 0.25° × 0.25° (WGS 84); and can be freely downloaded after registration on the CCI SM Website.

2.1.5. ISMN in situ data

The International Soil Moisture Network (ISMN) was initiated in 2009 in order to support the calibration/validation (cal/val) activities of remotely-sensed SM retrievals (Dorigo et al., 2011; Dorigo et al., 2013). More specifically, it was supported by ESA in the framework of the SMOS mission to help in the cal/val activities. Once in situ SM observations are collected from international networks, they are quality controlled and harmonized to be distributed through the ISMN website portal: https://ismn.geo.tuwien.ac.at/. Currently, the ISMN database hosts ground-based SM measurements from about ~58 networks located all over the world. Some of these datasets (e.g., SCAN, the US Climate Reference Network) are provided in near-real time. The in situ SM networks used in this study during the 2010–2017 period are listed in Table S1 and displayed in Fig. S1, covering a variety of climate and vegetation conditions (see Supplementary materials) but not all ecosystems are equally well represented. In this study, only SM observations flagged as "Good" were considered in the evaluations (Dorigo et al., 2013). In addition, OZNET and AMMA networks datasets were obtained from http://www.oznet.org.au/mdbdata/mdbdata.html and T. Pellarin (personal communication), respectively. Some networks have their stations distributed over an area that is smaller than the typical footprint of the space borne instruments considered in this study. This results in samples that are not independent in the comparisons, but this was not considered as a problem because the effect is largely the same for each product.

2.2. Methodology

The satellite SM products were evaluated against ground-based measurements following two approaches i) using all available SM retrievals for each product within the period 2010–2017; ii) using common dates (i.e. days where all satellite-based SM observations are available) between the different datasets, either with or without including SMAP. Approach (i) is used assuming that the final users of SM products may use these products separately, and hence limiting the evaluation to common dates may not correspond to the actual accuracy which will be obtained by the end user. SMAP is available for a shorter period compared to the other products, and was therefore either included or excluded in approach (ii) to evaluate the influence of time series length and data sampling in the evaluation. All products used in this study were provided in "a daily time step", therefore, in all these cases the instantaneous overpass times, for each day, were matched with instantaneous in situ measurements within a time window of 1 h. Dates with no match with in situ observations were not considered in the analyses. In addition, stations with a number of data pairs lower than one month (~31) were excluded from the analyses (e.g., Kolassa et al., 2018). Finally, stations where all remotely-sensed SM products obtained Pearson correlation values (R) < 0.5 were screened out.

Four scores, widely used by the SM community, were used here to evaluate the remotely-sensed SM products: Pearson correlation coefficient (R; Eq. (2)) to evaluate the ability of satellite-based retrievals on capturing SM seasonal variations of in situ measurements, Bias (Eq. (3)) to measure the dryness or wetness of the satellite-based retrievals compared to in situ observations, RMSE (Root mean square error; Eq. (4)), and the unbiased RMSE (ubRMSE; Eq. (5)) given as follows:

$$R = \sqrt{1 - \frac{(SM_{RS} - SM_{REF})^2}{(SM_{RS} - \overline{SM_{REF}})}} \quad (2)$$

$$Bias = \overline{(SM_{RS} - SM_{REF})} \quad (3)$$

$$RMSE = \sqrt{\overline{(SM_{RS} - SM_{REF})^2}} \quad (4)$$

$$ubRMSE = \sqrt{RMSE^2 - Bias^2} \quad (5)$$

where SM_{RS} is the satellite-based SM, SM_{REF} is the ISMN in situ SM used as a reference, and the temporal mean of the entire time series is indicated by an overbar.

The ground-based measurements are based on in situ observations at single location. Therefore, the in situ data have a spatial support that differs largely from the gridded SM retrieval products, which themselves are derived from elliptical footprints. The problem is all the more complex for SMOS, as (i) SMOS retrievals are based on multi-angular observations, and (ii) the available range of the SMOS observations over a given pixel changes from one date to the other (with a sub-cycle of about 16 days). Consequently, all metrics will be prone to representativeness error (Gruber et al., 2019, in preparation). These errors have been earlier analyzed, for example, by Crow et al. (2012) and

Famiglietti et al. (2008). These studies showed that the representativeness errors significantly affect the reliability of the metrics in the absolute sense. However, the analysis presented here is comparative in nature and while the representativeness errors also degrade the ability of the comparisons to detect differences between the products, the results carry information on relative merits of the products. Alternative approaches that may mitigate this problem for sparse networks include deployment of triple collocation technique (for example, Chen et al., 2017a), but this is outside of the scope of this study. Moreover, the sampling depth can be different among satellites and among in situ sensors thus leading to mismatch in soil depth, which can potentially affect the evaluation. OZNET network, for instance, measures SM within the 0–5 cm topsoil layer, while most of the other networks measure SM at 5 cm.

Furthermore, the SM seasonal cycle was removed by computing R using anomalies (R_{anom}). This is to evaluate the ability of satellite-based SM retrievals on capturing the day to day variability (short variations) of in situ SM observations, which is more important than absolute values for many applications (e.g. data assimilation) and which also reduces part of the representativeness issue mentioned above. The anomaly was computed using the following formula (e.g., Parrens et al., 2012; Rodríguez-Fernández et al., 2016):

$$SM_{anom} = \frac{SM_i - \overline{SM\ (w)}}{SD\ (SM\ (w))} \quad (6)$$

where SM_i is the SM value at day (i) and $\overline{SM\ (w)}$ and SD (SM (w)) are the mean and standard deviation over a sliding window (w) of 35 days (Albergel et al., 2012; Brocca et al., 2011), respectively. Note that the seasonalities are not averaged across years into a climatology.

SM time series were extracted from the original grids (e.g., 36 km for SMAP, 25 km for SMOSL3, etc.) from those pixels that correspond to each station separately (based on its latitude and longitude). This being said, it is likely that some stations from a dense network (e.g., OZNET) may correspond to the same passive (SMAP, SMOS, and CCI) pixel but for several active (ASCAT) pixels. Then, the metrics between satellite data and the in situ observations were computed separately for each station. Finally, the median of each metric for all stations within a continent was calculated. In addition, the median of each metric for all stations within a land cover type (derived from MODIS (Friedl et al., 2010)), LAI category, or Köppen-Geiger climate zone (Rubel et al., 2017), displayed in Fig. S1 (in the Supplementary), was also computed and presented in the following section. Correlation coefficients (R) are not additive measures and thus cannot be simply averaged; therefore, the median was instead computed. The spatial standard deviation is added to the median skill metrics.

3. Results

3.1. Using all available observations

The four scores (R, Bias, RMSE, and ubRMSE) were computed between remotely-sensed SM retrievals (if available) and 17 ISMN in situ observation networks listed in Table S1 in the Supplementary. As mentioned before, all observations available within the 2010–2017 period were considered. This being said, the period used to compute the scores for each product can be different.

Fig. 1 shows the overall performance (R, R_{anom}, Bias, RMSE, and ubRMSE scores) of each product stratified by continent. For stations located in Africa, ASCAT had overall slightly higher correlation values but also higher Bias, RMSE, and ubRMSE values than all other SM products. Nonetheless, there are small differences in terms of R between the remotely-sensed SM products (R ranging from ~0.75 to ~0.80). Therefore, temporal SM variations from in situ stations over sites in this continent are well reproduced by the remotely-sensed SM products. However, R_{anom} dropped for all the remotely-sensed SM products with higher and similar performances by SMAP and SMOS-IC. Over this region, all products were wetter than the in situ observations (consistent with Al Bitar et al. (2017) for SMOS V300 and Rodríguez-Fernández et al. (2016) for ESA CCI V2.02 SM).

For the U.S. networks (e.g., SCAN, SNOTEL, SOILSCAPE, USCRN, etc.), SMAP had the highest correlation (followed by SMOS-IC), lowest ubRMSE and RMSE values (followed by CCI). In terms of R_{anom}, SMOS-IC had the highest value, whereas the other five products had similar performances. All data sets were drier than the ISMN observations with the highest Bias values obtained by SMOS-IC.

For the Australian network (OZNET), while SMOS-IC and CCI had the lowest ubRMSE (followed by SMOSL2 SM) and RMSE values, SMAP and SMOS-IC had the highest correlation (original and anomalies) values along with SMOSL2 and SMOSL3. All products were wetter than the in situ observations. The results over the OZNET network are consistent with Colliander et al. (2017) who also showed, for instance, that SMAP is wet (although the study was based only on data of the Yanco site and used SMAPL2 V2).

In case of the European networks (e.g., REMEDHUS, SMOSMANIA, BIEBRZA_S-1, RSMN, HOBE, etc.), ESA CCI SM had the lowest overall ubRMSE (followed by SMAP) and RMSE values, while SMAP and SMOS-IC showed the highest values in terms of correlations. SMOS-IC, again, had the highest R_{anom} values. There is a strong variability in terms of Bias for the different products: from an underestimation by all SMOS products to an overestimation by SMAP, ASCAT and the ESA CCI SM.

Generally, the best performance of all remotely-sensed SM products was found over Australian and African stations, while the worst and diverse results were found over the U.S. and Europe. Remarkably, a systematic overestimation or underestimation of the ISMN in situ observations has been observed by remotely-sensed SM products over stations located over Africa (and Australia) and America, respectively. Generally, for areas without or with very few RFI (Australia and Africa) SMOS had positive biases but when there are many (Europe) it is always negative (Bircher et al., 2012). It should be noted that some areas are much better represented than others (US vs Africa for instance) in terms of number of points and that for Africa only one ecosystem is considered ranging from temperate to arid via tropical.

3.2. Using only temporally collocated data

3.2.1. For the SMAP period (Jan 2015–Dec 2016)

Here, we limited the analyses to only common dates by doing a temporal collocation between the different satellite-based SM retrievals (Fig. 2). Due to the short period of SMAP, only 9 networks out of 17 were retained: OZNET, PBO_H2o, REMEDHUS, RSMN, SCAN, SMOSMANIA, SNOTEL, SOILSCAPE, and USCRN. As expected, the rank of the product performances in Fig. 2 is different to the one shown in Fig. 1 (without temporal collocation).

Over the U.S. networks (North America), SMOS-IC, SMOSL2, and SMAP (ASCAT) had the highest (lowest) correlations (both original and anomalies). There is almost similar performance in terms of R and RMSE values between SMOSL2, SMOS-IC and SMAP but lowest (highest) ubRMSE was obtained by SMAP (SMOSL3 and ASCAT). All products (except for ESA CCI SM, whose bias is the model bias of GLDAS Noah) are drier than the in situ observations; with, again, marked underestimation by SMOS-IC as already seen in Fig. 1. Lower R_{anom} values were obtained by all products but the performance rank of the products was unchanged.

Over the Australian network (OZNET), all SMOS versions and SMAP had almost similar performance in capturing the temporal dynamics (both annual cycle and day to day variations) of the ISMN in situ observations and better compared to in situ observations than ESA CCI SM and ASCAT SM products. SMOS-IC and SMOSL3 (SMAP) had the lowest (highest) ubRMSE values. All SMOS products had similar RMSE values and lower than the other products. All remotely-sensed SM products were wetter than the in situ measurements (with the exception of SMOS-IC).

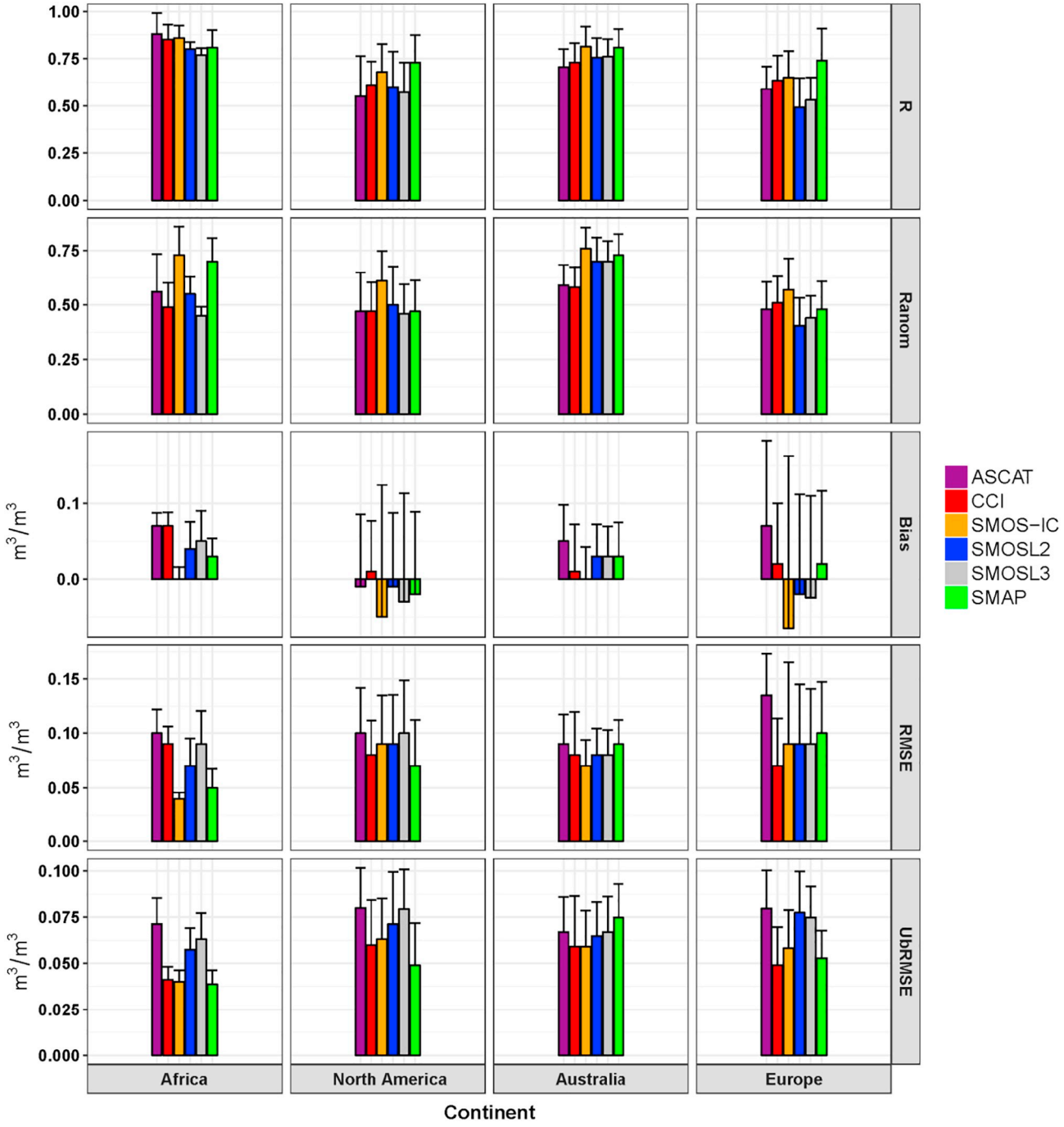

Fig. 1. Median evaluation metric (R, R_{anom}, Bias, RMSE, and ubRMSE) for the entire period 2010–2017, across all sites for all products (without data cross masking) compared to ISMN in situ SM, stratified by continent: America (n = 448 stations), Australia (n = 46 stations), Europe (n = 128 stations), and Africa (n = 13 stations). Error bars represent the standard deviation (SD; variability) of the station metrics (median + SD) and do not represent anything on the temporal sampling frequency.

In case of Europe, there is generally no big difference in terms of correlations between the products but strong differences can be noted in terms of UbRMSE and Bias. SMOS-IC and ASCAT had the highest R_{anom} values against the ISMN observations. Similarly to what was already found in Fig. 1, while all SMOS SM products were drier than the in situ measurements, ESA CCI SM and ASCAT were wetter than the in situ measurements.

3.2.2. For the period without SMAP (Jan 2010–Dec 2016)

Excluding SMAP, only SMOS, ESA CCI, and ASCAT SM products were considered. Here, fourteen in situ SM networks were retained: AMMA, ARM, BIEBRZA_S-1, DAHRA, HOBE, OZNET, PBO_H2O, REMEDHUS, RSMN, SCAN, SMOSMANIA, SNOTEL, SOILSCAPE, and USCRN. As done in Figs. 1 and 2, Fig. 3 shows the overall performance of the remote-sensing SM products stratified per continent.

In the case of sites located over Africa, there are generally strong correlations between satellite-based SM products and the in situ observations with similar performances in terms of correlations (R) - with the exception of SMOSL3- and lowest ubRMSE values were obtained by SMOS-IC and ESA CCI SM products. As over America and Europe, no change in terms of Bias from Fig. 1 was found. It should be noted that SMOSL2 outperformed SMOSL3 in most scores, which is in line with the

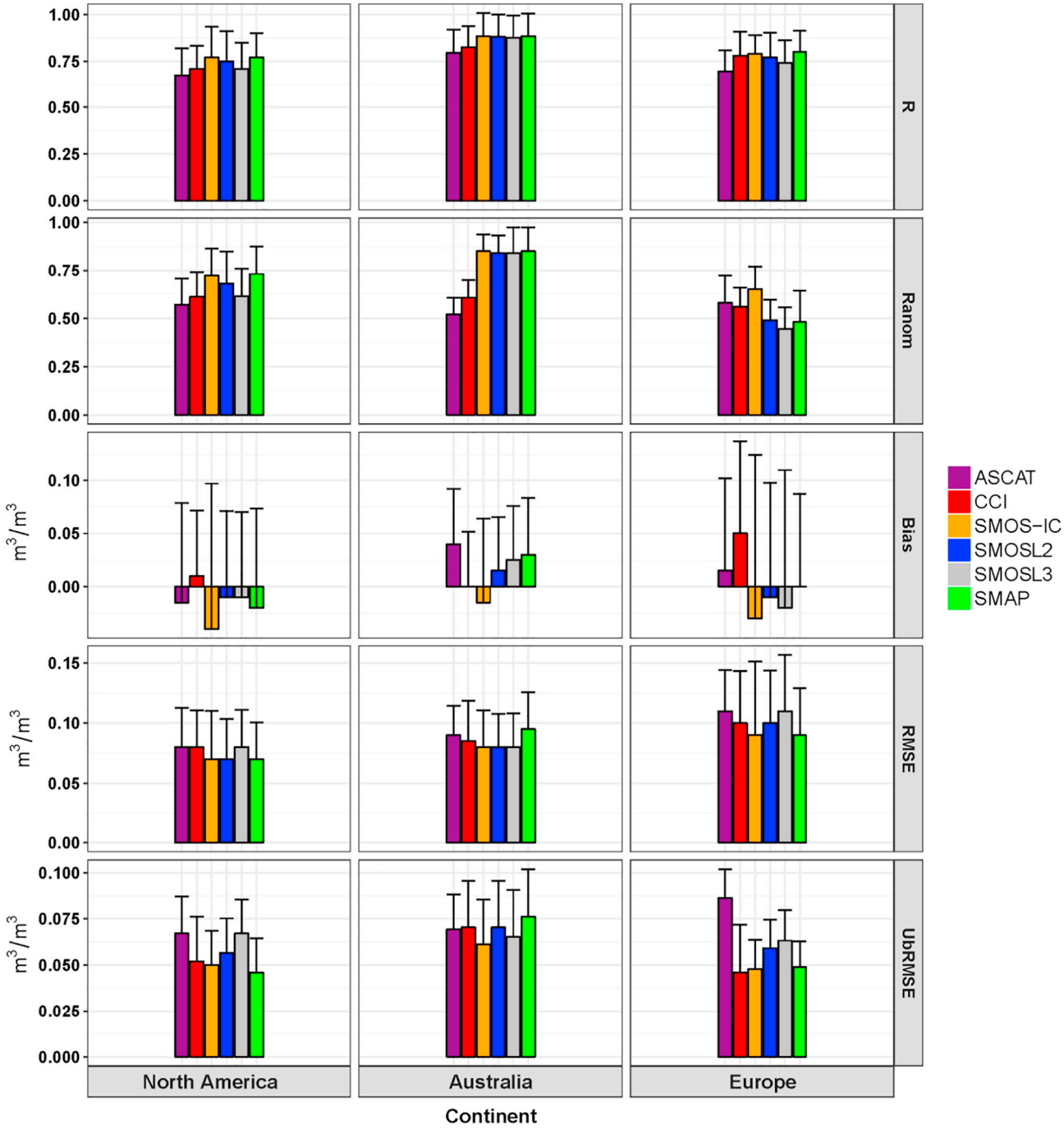

Fig. 2. Same as Fig. 1, but now only including common data points for each product within the 2015–2016 period, and hence using a reduced number of stations (n) over North America (n = 174 stations), Australia (n = 30 stations), and Europe (n = 27 stations).

findings of Al Bitar et al. (2017), using SMOSL2 V620 and SMOSL3 V300.

For the U.S. networks, SMOS-IC (followed by SMOSL2 and ESA CCI) presented slightly higher correlation values. SMOS-IC and SMOSL2 presented higher R_{anom} and the other three products performed similarly. As found in Fig. 1, all data were drier than the in situ observations except ESA CCI SM which is wetter, with again marked underestimation by SMOS-IC. Similar and lower RMSE values were obtained by ESA CCI, SMOSL2, and SMOS-IC. Similar and lower ubRMSE values were obtained by ESA CCI and SMOS-IC.

Over the Australian network, the highest correlation values (R and R_{anom}) were obtained by SMOS-IC, SMOSL2, and SMOSL3. The lowest ubRMSE value was obtained by SMOSL2. In general, over Australia, the SMOS SM products perform better than the ESA CCI SM and ASCAT (in line with the findings of Holgate et al. (2016)) products but there are small (or no) differences between the SMOS products and the ESA CCI SM products in terms of RMSE and ubRMSE values with SMOSL2 product being the best for UbRMSE and SMOS-IC for RMSE. No change in terms of sign of Bias from Fig. 1 (although the magnitudes are different).

In the case of sites located over Europe, SMOS-IC (followed by ESA CCI SM and ASCAT), again performed slightly better in terms of correlations (R and R_{anom}) than the other products but the lowest ubRMSE values were obtained by ESA CCI SM. Lowest RMSE values were obtained by ESA CCI, SMOSL3, and SMOSL2. No change in terms of sign of Bias can be noted in comparison to Fig. 1.

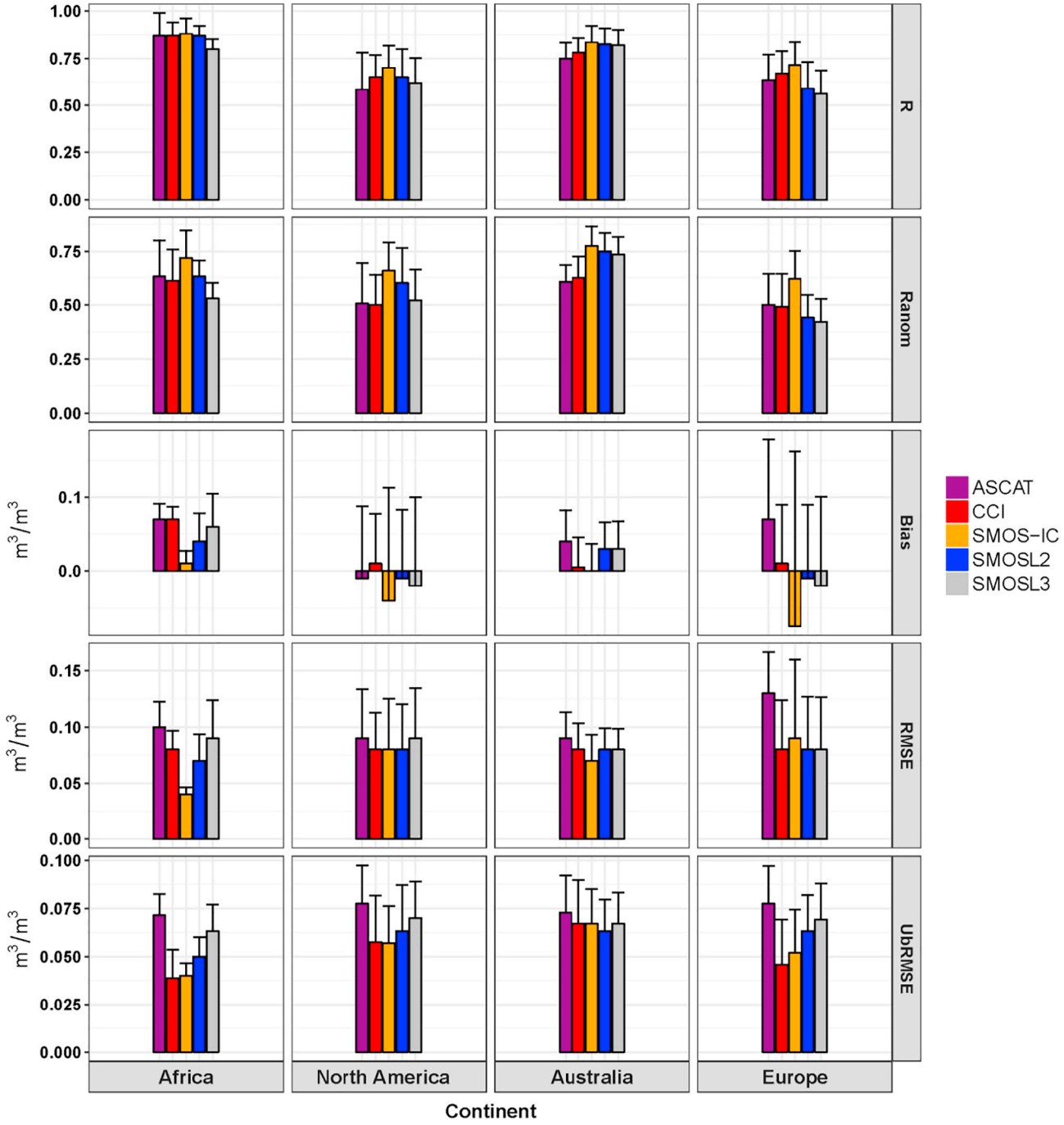

Fig. 3. Same as Fig. 2, but now excluding SMAP and extending the evaluation period to common data points in 2010–2017, over North America (n = 393 stations), Australia (n = 28 stations), Europe (n = 94 stations), and Africa (n = 13 stations).

3.3. Impact of vegetation and climate

For the ISMN networks used in this study, climate and land cover can be quite heterogeneous in some continents (e.g. North America and Europe) and relatively homogeneous in others (e.g. Australia and Africa). So in this section we analyze more in depth the impact of vegetation and climate on the performances of the satellite-based SM products.

3.3.1. Vegetation

There is consensus among the SM community that vegetation density affects the remotely-sensed SM quality (Jackson et al., 1982; Wigneron et al., 2017). Earlier studies (e.g., Al-Yaari et al., 2014a; Al-Yaari et al., 2014b) found that the performance of the satellite-based SM products varies depending on the vegetation density and land cover type. This section is devoted to re-evaluate the impact of vegetation on the performance of SM products using new SM versions/products. Given the fact that all SMOS products (i.e. SMOS-IC, SMOSL3, and SMOSL2) use SMOS TB observations and ECMWF soil temperature data, they are not totally independent. Also, there is slightly better performance of SMOS-IC over the other SMOS products. Therefore, to simplify the inter-comparison, this section is limited to the SMOS-IC version and other none-SMOS products. The evaluation scores (for all stations) i.e. R, R_{anom}, Bias, RMSE, and ubRMSE are stratified based on the IGBP land cover type (see Fig. S1 in the Supplementary). Results, based only on common dates within the period 2015–2016 (2 years), are displayed in Fig. 4.

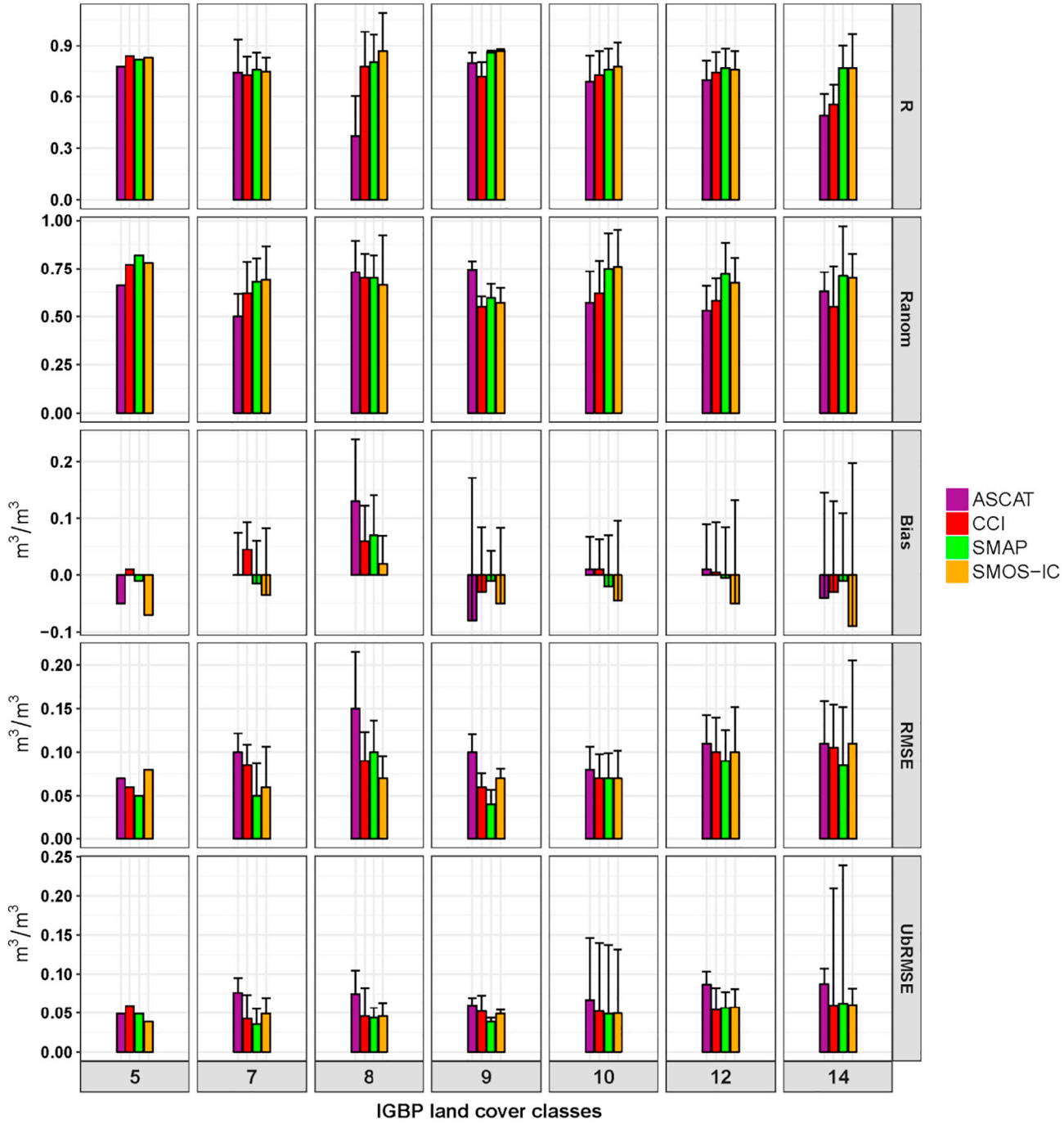

Fig. 4. Median metrics (R, R_{anom}, Bias, RMSE, and ubRMSE) of all sites stratified by IGBP land cover type (see Fig. S1) for SMOS-IC, ASCAT, CCI, and SMAP: Mixed forest (5; n = 1 station), Open shrublands (7; n = 10 stations), Woody savannas (8; n = 8 stations), Savannas (9; n = 27 stations), Grasslands (10; n = 132 stations), Croplands (12; n = 67 stations), Cropland/Natural vegetation mosaic (14; n = 22 stations). n denotes the number of stations per land cover type. Error bars represent the standard deviation (SD; variability) of stations (median + SD). Only data points at common dates within the period 2015–2017 are included.

In terms of correlation (R), similar performances between the four products (SMOS-IC, ESA CCI SM, ASCAT, and SMAP) were found over "Open shrublands", "Croplands", and "Mixed forest". A notable difference between ASCAT (lower performance) and the other three products was found over "Woody savannas". SMOS-IC and SMAP had best correlations with the ISMN observations over "Cropland/Natural vegetation mosaic". SMAP and SMOS-IC had the highest anomaly correlations over "Grasslands" and "Croplands". ASCAT was correlating better to in situ measurements anomalies over "Savannas". All the four products agree in terms of sign of the bias value: while all underestimated the ISMN observations over "Cropland/Natural vegetation mosaic" and "Savannas", they all overestimated the ISMN observations over "Woody savannas". However, there is no agreement between products in terms of sign of the bias over all other land cover types. In terms of RMSE and ubRMSE, while ASCAT had generally the highest values, the other three SM products performed similarly over most of the land cover types.

A different insight on the impact of vegetation on the performance of satellite-based SM retrievals with respect to the ISMN in situ observations can be seen in Fig. 5. Fig. 5 displays the median of all the statistics considered in this study stratified based on MODIS LAI categories: 0–1, 1–2, and 2–3 m^2/m^2 (see Fig. S1 for the MODIS LAI map). Evidently, because the prior data masking to locations with < 5 kg/m^2

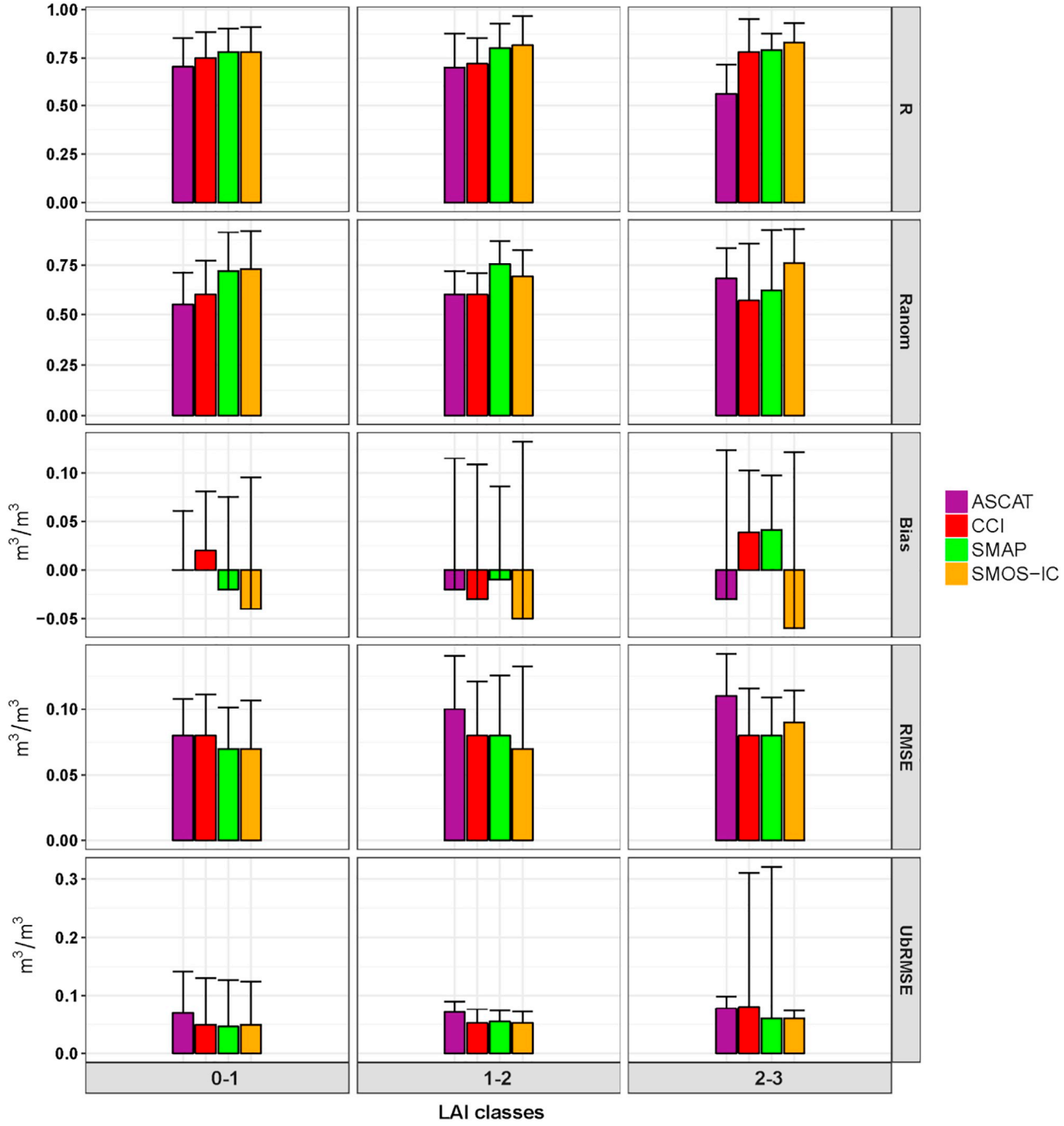

Fig. 5. Same as Fig. 4, but now grouped by LAI values in 3 classes: 0–1, 1–2, 2–3 m^2/m^2. Number of stations per category: 0–1 (n = 160 stations), 1–2 (n = 99 stations), 2–3 (n = 9 stations).

VWC, only limited data are available for evaluation in densely vegetated areas. It can be noticed from this figure that there is an increase in ubRMSE for all remotely-sensed SM products with increasing vegetation density. For SMAP and ESA CCI there is a high variability of their performances among stations as indicated by the high standard deviation over the LAI 2–3 category. In terms of R, similar performances among products can be noticed over the category 0–1 but better performance was obtained by SMOS-IC going from 0–1 to 2–3 categories, whereas ASCAT retrievals degraded for denser vegetation. The best R_{anom} values were obtained by SMOS-IC (followed by ASCAT) and SMAP (followed by SMOS-IC) over the 2–3 and 1–2 categories, respectively. SMOS-IC and SMAP performed similarly in terms of R_{anom} over the 0–1 category. In terms of ubRMSE, none is superior over all LAI categories. For instance, while SMAP, SMOS-IC, ESA CCI SM products had similar ubRMSE values over regions with LAI values ranging between 0 and 2 m^2/m^2, SMOS-IC and SMAP had lowest values over the LAI 2–3 category. The four products only agree in terms of sign of bias (dry) over LAI 1–2 category and higher Bias values were obtained by SMOS-IC.

3.3.2. Climate

Climate is another factor that can impact the performance of the remotely-sensed SM products. In this study, we assessed the relationship between satellite performance metrics and the Köppen-Geiger climate classification (Kottek et al., 2006). Fig. 6 displays the median of all the statistics considered in this study as a function of Köppen-Geiger

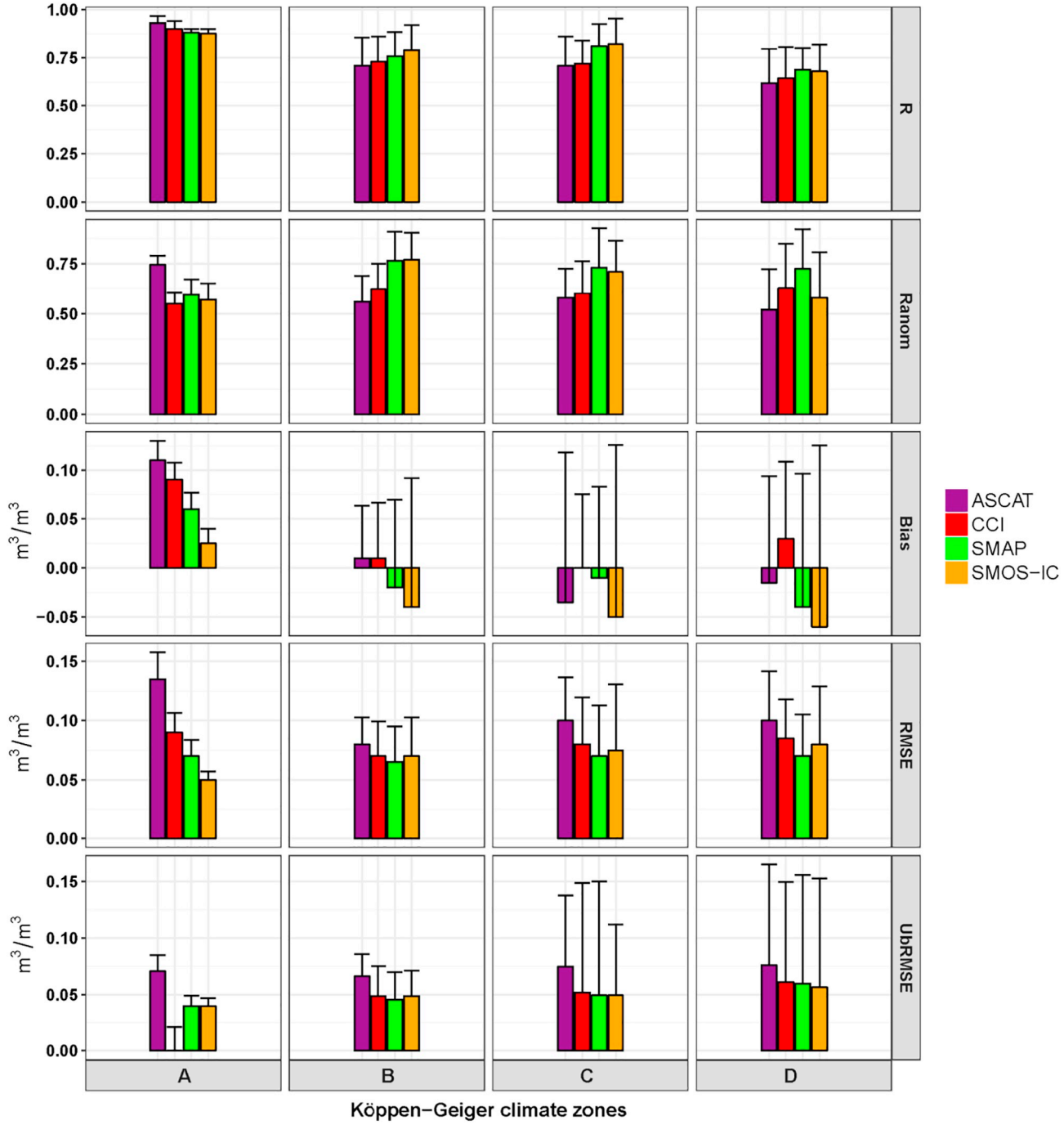

Fig. 6. Same as Fig. 4, but now grouped by Köppen-Geiger main climates (see Fig. S1). A: Equatorial (Savanna; n = 8 stations), B: Arid and semiarid (n = 90 stations), C: Warm temperate climates (n = 132 stations), D: Cold climates (n = 42 stations). Source of the climate classifications: (Kottek et al., 2006).

main climates (see Fig. S1 for the Köppen-Geiger map): "Equatorial (Savanna) climates: (A)", "Arid and semi-arid climates (B)", "Warm temperate climates (C)", and "Cold climates (D)". It can be noticed from this figure that there is a high variability in the performance of the satellite-based products over regions classified as "B", "C", and "D" in terms of Bias. All remotely-sensed SM products have comparable performances (with small differences) in terms of correlations over "A", "B", and "D" climates in terms of R. The lowest correlations and highest RMSE and ubRMSE values for all products were obtained over "cold climates" climate. SMAP and SMOS-IC correlated better to the ISMN observations over "warm temperate climates" climates than ESA CCI and ASCAT. ASCAT had higher RMSE and ubRMSE over all the main climates and lower R_{anom} over "B", "C", and "D". However, ASCAT had higher correlations (both original and anomalies) over "Equatorial (Savana) climates". The correlations values computed based on anomalies were lower than the original ones particularly over "Equatorial (Savana) climates" and the performance is more spread over the stations. SMAP had a higher R_{anom} over "cold climates" but comparable with SMOS-IC over "Arid and semi-arid climates" and "warm temperate climates" and with SMOS-IC and CCI over "Equatorial (Savana) climates". In terms of anomalies, the rank of the products did not change over "Arid and semi-arid climates". With the exception of CCI, remotely-sensed SM products had underestimated in situ observations over "warm temperate climates" and "cold climates" and overestimated the ISMN SM observations over "Equatorial (Savana) climates". With the exception of ASCAT, all products had comparable ubRMSE values

over “B”, “C”, and “D” regions. Moreover, “Arid and semi-arid climates” region exhibits high variability in terms of performance scores.

4. Discussion

Based on the evaluation results shown above in Figs. 1–3, it was found that comparing remotely-sensed SM product to the ISMN in-situ measurements individually (i.e. taking all available observations) or limiting observations to the availability of the other remotely-sensed SM products can impact the evaluation scores and the ranking of the various SM retrieval products, due to differences in spatial and temporal sampling. On the one hand, considering all observations, SMAP and SMOS-IC gave the best performance in terms of correlations (Fig. 1), while on the other hand, they had similar performance to SMOSL2 and SMOSL3 when considering only common dates over the Australia network (Fig. 2). Another example concerns stations situated over Africa, where ASCAT provided the highest correlation value (though the differences were small) when considering all observations (Fig. 1) but when considering only observations collocated with the other products, a similar performance with CCI, SMOSL2, and SMOS-IC (Fig. 3) was obtained.

In some cases, the performances were unchanged when cross masking data. This may be coincidence, or it may indicate that the masked data are indeed a representative subsample of all data. For instance, in terms of ubRMSE, ESA CCI SM was the best in all cases over Europe. SMOS-IC was the best for ubRMSE and this position was unchanged whether all observations were considered (Fig. 1) or considering only common dates (Fig. 2) over the Australian network. All remotely-sensed SM products (except SMOS-IC) were consistently wetter than the ISMN SM products over the African and Australian networks in all cases considered in this study i.e. using all observations or only common dates. Similarly, the small bias in dryness (wetness) of ASCAT, SMAP, and SMOS (ESA CCI SM) with respect to the ISMN observations over stations located in the U.S. persisted, regardless of the data masking. The dryness of SMAP is in line with previous studies conducted by Chen et al. (2017b), over the Tibetan Plateau. The presence of bias is a common problem of the remotely-sensed SM products analyzed in this study. Other than the representativeness errors between the point-scale in situ measurements and coarse-resolution space borne products, the absolute value of Bias is affected by (Al Bitar et al., 2017; Draper et al., 2009; Escorihuela et al., 2010; Jackson et al., 2012): different sensing depths (and thus observed volume), the use of auxiliary variables from models (e.g., soil temperature), uncertainties due to the in situ sensor errors, scaling and conversion of units (mainly for ESA CCI SM and ASCAT), and spatial heterogeneity.

Overall, the ubRMSE values are larger than the target uncertainty of 0.04 m^3/m^3 when doing an evaluation against sparse networks, which suffer largely from representativeness error. It is worth noting that the ubRMSE values (particularly for SMAP) found in this study are in line with those found by El Hajj et al. (2018), but larger than those found by Colliander et al. (2017) and Chan et al. (2016). These later studies used core validation sites, which have significantly smaller representation errors through upscaling of the dense SM networks; here we considered the median value of the scores of individual stations within continents, land cover types, or climate zones. Furthermore, it was shown that ASCAT generally had the highest ubRMSE values compared to other products over most of the networks and lower correlations over arid environments. This could be explained by volume scattering in dry sands and the fact that the ASCAT product is given as a degree of saturation unit, which was converted to the volumetric units (i.e. m^3/m^3) using soil porosity information (Wagner et al., 2013). Soil porosity datasets are often not very accurate (Brocca et al., 2011), and they may significantly affect the Bias and ubRMSE scores obtained by ASCAT. In addition, it should be noted that the Bias values obtained for the ESA CCI are imposed by the GLDAS Noah model, as already mentioned above.

The increase in R values when only common data points are used is most likely because less stations are included, which each now has a more complete time series, allowing to sample more of the long-term variability. When excluding SMAP from the analyses (Fig. 3), SMOS-IC generally (followed by SMOSL2 and ESA CCI in most cases) ranked first in terms of correlations (both original SM values and anomalies) for most of the ISMN stations considered in this study. However, the differences in R values are rather very small. The slightly better performance of SMOS-IC is probably due to the improvements introduced into the algorithm (e.g., limiting the use of auxiliary information, new calibration, etc.). However, SMOS-IC showed higher Bias values comparing to other products which is expected as Bias was considered as the least important metric in the SMOS-IC SM algorithm calibration processes (Fernandez-Moran et al., 2017a).

While the best performances of all remotely-sensed SM products in terms of correlation were found over the Australian and African networks (due to common low vegetation density over these networks), the worst and more diverse results were found over the European networks (particularly SMOS). However, in most cases and particularly for stations located over Africa, anomaly correlations were lower than for the original correlations, which means that the correlations of those stations were controlled by the annual cycle (pronounced dry and wet seasons). In the case of Europe, the SMOS observations are affected by RFIs plus snow freezing not always well taken into account (partial coverage, human impacts) that could partially explain the lower performances of SMOSL2 and SMOSL3 over this continent.

As RFIs signals play a key role in the accuracy of the SM products retrieved from the passive microwave systems, we further analyzed the impact of this factor in Fig. 7 for the SMOS sensor (times series of observations were too short for the SMAP data which are not included in this analysis). More specifically, the time variation in the quality of the SMOS SM product since 2010 was investigated over the four continents: America, Australia, Africa, and Europe. The correlation values shown in Fig. 7 (upper panel) were calculated for each year separately between the SMOS-IC and ISMN data and then only the median of all sites per continent and year was retained. In Fig. 7 (upper panel), it can be seen that the performance of SMOS-IC over America is stable with no substantial differences between years. Over Australia and Europe (except for 2015), there is a small tendency of increasing correlations from 2010 onwards. Over Africa, there is no obvious trend as the performance of SMOS-IC changes from one year to the other. In order to investigate the effect of RFI on the SMOS-IC results in Fig. 7 (upper panel), the temporal mean of the RMSE of the fit between measured and simulated TB (which can be considered as a proxy of RFI impacts on the TB observations) was computed per year and spatially averaged for the same corresponding entire continents; displayed in Fig. 7 (lower panel). While a substantial decrease in RFI can be noticed over America, RFI over Australia keeps stable through the seven years. Over Africa and Europe, RFI signals effects changed from one year to the other with no general trends. Interestingly, the notable decrease in the performance of SMOS-IC over 2013–2014 over Africa and 2015 over Europe corresponds to higher RFI levels than in the preceding and following years. So, these figures tend to confirm that the RFI effects may be a key factor to explain time variations in the performance of SMOS-IC over these continents. The lowest RFI signals among continents were found over Australia, which was reflected in the best performance of SMOS-IC in all years in terms of correlations over the continents. The results showed that the performance of SMOS datasets is still highly affected by RFI signals, even if ESA already put a lot of efforts in closing down many RFI sources (Oliva et al., 2016). However, this cannot be generalized as for instance over Europe, the TB RMSE decrease in 2011 (lower RFI conditions) matches with an R-decrease in SM.

Other general disturbing factors that impact the performance of the remote sensing SM products over Europe include climate, dense vegetation, or mountains. The regions of SM networks over the African and Australian networks are relatively homogenous with less spatial

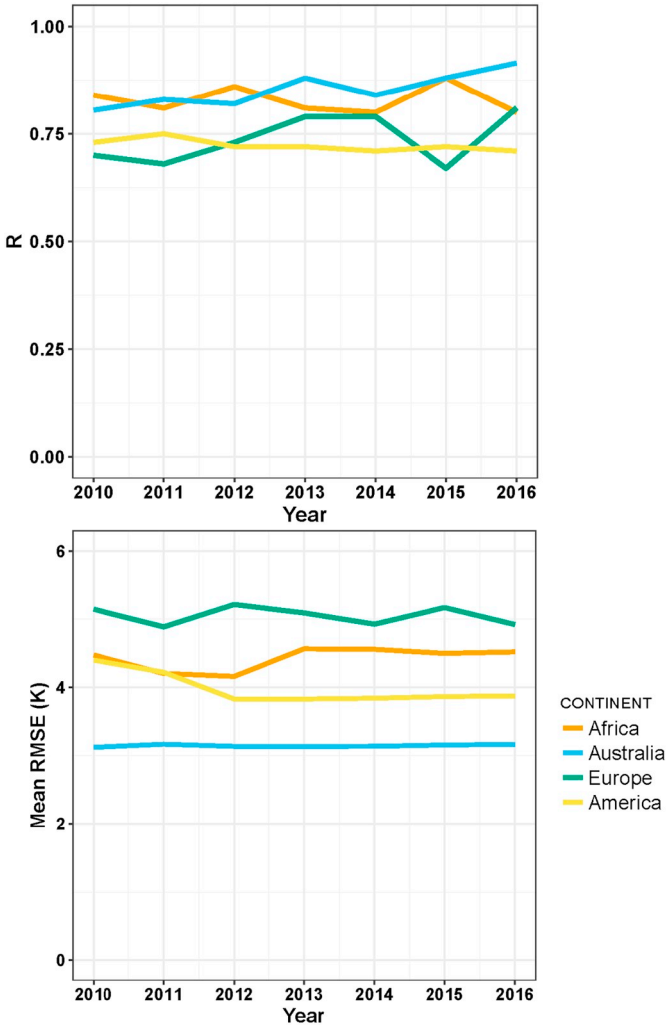

Fig. 7. Correlation between SMOS-IC SM and the ISMN in situ SM observations (upper panel) and RMSE of the fit between measured and simulated TB (bottom panel) during the 2010–2016 period over Africa, Europe, America, and Australia. Correlations were calculated per year separately for all stations located in the same continent and then the median of all stations was computed.

variability in SM, which led to higher skills of remote sensing retrievals (e.g., Dorigo et al., 2012). In terms of correlations and ubRMSE: while lowest performances (with more variability) of most the remotely-send SM products were obtained for "cold climates", which is expected due to the effects of snow and frozen conditions that are not well filtered or the landscape (vegetation, soil) is very different from the other areas where much of the algorithm development has occurred. Highest performances were obtained over "tropical savanna climates", which is, as mentioned above, mainly controlled by the annual cycle. This indicates that climate and the time series length is a significant factor when comparing satellite-based SM products.

The better performance, particularly in terms of temporal dynamics, of SMAP and SMOS-IC over active (ASCAT) products, using only common dates, over regions where LAI range between 2 and 3 m^2/m^2 is probably due to the fact that SMAP and SMOS (and ESA CCI which contains SMOS) operate at L-band which is optimal for SM monitoring: L-band observations have higher penetration capabilities through dense vegetation and lower sensitivity to atmospheric effects such as heavy rainfall events than higher frequencies (C- and X-bands). However, over these regions, ASCAT showed similar R_{anom} as SMAP. Over some land cover types/regions, the ESA CCI SM product was performing similarly to SMOS-IC and SMAP, which is probably due to the fact that it contains SMOS L-band observations. The small difference in correlation values (both R and R_{anom}) between SMOS-IC (higher) and SMAP (lower) over regions where LAI values range between 2 and 3 could be due to the capability of SMOS satellite to measure TB at multi-angular incidence angles and thus better decouple between the soil and vegetation effects. Conversely, the better performance, mainly in terms of ubRMSE of SMAP over the SMOS products is generally due to the improved technology used in SMAP (SMAP has a much better RFI filtering).

5. Conclusion

In this study, the assessment and inter-comparison of six recently developed/reprocessed satellite SM products (i.e. SMOS-IC, SMOSL2, SMOSL3, SMAP, ASCAT, and ESA CCI SM) against the ISMN ground-based measurements across different climate and vegetation conditions were conducted. This was accomplished using the Pearson correlation coefficient (R), anomalies (R_{anom}), Bias, RMSE, and ubRMSE metrics. Several conclusions can be drawn from the evaluation presented above:

(i) The performance of the six datasets in terms of correlations (temporal dynamics) was rather similar over contrasted biomes and climate conditions, but with a slightly higher skill of both SMAP and SMOS-IC products especially when the data were temporally collocated;
(ii) The performances of SM products related to systematic and random errors (i.e. Bias and ubRMSE) varied strongly between products and locations, but with a slightly higher skill of ESA CCI SM, SMOS-IC, and SMAP products. More specifically, similar performances in terms of dryness or wetness with respect to in situ observations were obtained over Australia and North America, with the exception of ESA CCI SM, regardless of the period or temporal collocation. The six products did not agree in the sign of the Bias over Europe in all of the analyses presented above. Bias strongly depends on the reference data sets and/or model parameters used to determine the absolute SM conditions such as porosity data for ASCAT or GLDAS Noah model for the ESA CCI SM products. Further research on teasing out and quantifying systematic errors in satellite-based SM retrievals should be recommended for the future;
(iii) When excluding SMAP from the analyses, SMOS-IC was correlating best to the ISMN in situ observations and both ESA CCI SM and SMOS-IC presented the lowest ubRMSE values;
(iv) The performance of SMOS-IC, in particular, seems highly impacted by RFI (which is not the case for SMAP or to lesser extent) as indicated by the decrease in correlations values for higher continent-averaged RFI values. RFIs may also to some extent influence the ESA CCI product which integrates both SMOS and AMSR-E/2;
(v) While the best performance (i.e. a better range of correlation values) of all remotely-sensed products was found for stations located in Australia and Africa (semi-arid environments), the worst and more diverse performances were found over Europe (particularly SMOS) and cold climates; and
(vi) A complementarity between ASCAT, SMOS, ESA CCI SM, and SMAP satellite-based SM products was demonstrated in this study given the none superiority of any of them and the different performances of each product over different land cover classes and climate conditions across the globe.

One should be very careful when trying to select the most skillful product, as the performance of each product varies based on the period of evaluation, the evaluation protocol, the data quality control, the number of data points and the study region. These factors could favor one of the products over the others, as it was demonstrated in this study, which makes it a challenge to draw firm conclusions. The SM community is actively working on establishing common guidelines (Gruber et al., 2019, in preparation) for evaluating satellite-based SM products, which should help future studies in the ranking of various SM

products for various applications.

Acknowledgements

This work was jointly supported by CNES, France (Centre National d'Etudes Spatiales) through the TOSCA (Terre Océan Surfaces Continentales et Atmosphère) program and the European Space Agency (ESA; SMOS Expert Support Laboratory).

Appendix A. Supplementary data

Supplementary data to this article can be found online at https://doi.org/10.1016/j.rse.2019.02.008.

References

Al Bitar, A., Mialon, A., Kerr, Y.H., Cabot, F., Richaume, P., Jacquette, E., Quesney, A., Mahmoodi, A., Tarot, S., Parrens, M., Al-Yaari, A., Pellarin, T., Rodriguez-Fernandez, N., Wigneron, J.P., 2017. The global SMOS level 3 daily soil moisture and brightness temperature maps. Earth Syst. Sci. Data 9, 293–315.

Albergel, C., Rüdiger, C., Carrer, D., Calvet, J.-C., Fritz, N., Naeimi, V., Bartalis, Z., Hasenauer, S., 2009. An evaluation of ASCAT surface soil moisture products with in-situ observations in Southwestern France. Hydrol. Earth Syst. Sci. 13.

Albergel, C., de Rosnay, P., Gruhier, C., Munoz-Sabater, J., Hasenauer, S., Isaksen, L., Kerr, Y., Wagner, W., 2012. Evaluation of remotely sensed and modelled soil moisture products using global ground-based in situ observations. Remote Sens. Environ. 118, 215–226.

Al-Yaari, A., Wigneron, J.P., Ducharne, A., Kerr, Y., de Rosnay, P., de Jeu, R., Govind, A., Al Bitar, A., Albergel, C., Muñoz-Sabater, J., Richaume, P., Mialon, A., 2014a. Global-scale evaluation of two satellite-based passive microwave soil moisture datasets (SMOS and AMSR-E) with respect to Land Data Assimilation System estimates. Remote Sens. Environ. 149, 181–195.

Al-Yaari, A., Wigneron, J.P., Ducharne, A., Kerr, Y.H., Wagner, W., De Lannoy, G., Reichle, R., Al Bitar, A., Dorigo, W., Richaume, P., Mialon, A., 2014b. Global-scale comparison of passive (SMOS) and active (ASCAT) satellite based microwave soil moisture retrievals with soil moisture simulations (MERRA-Land). Remote Sens. Environ. 152, 614–626.

Al-Yaari, A., Wigneorn, J.P., Ducharne, A., Kerr, Y., Fernandez-Moran, R., Parrens, M., Bitar, A.A., Mialon, A., Richaume, P., 2015. Evaluation of the most recent reprocessed SMOS soil moisture products: comparison between SMOS level 3 V246 and V272. In: 2015 IEEE International Geoscience and Remote Sensing Symposium (IGARSS), pp. 2493–2496.

Al-Yaari, A., Wigneron, J.P., Kerr, Y., Rodriguez-Fernandez, N., O'Neill, P.E., Jackson, T.J., De Lannoy, G.J.M., Al Bitar, A., Mialon, A., Richaume, P., Walker, J.P., Mahmoodi, A., Yueh, S., 2017. Evaluating soil moisture retrievals from ESA's SMOS and NASA's SMAP brightness temperature datasets. Remote Sens. Environ. 193, 257–273.

Bircher, S., Balling, J.E., Skou, N., Kerr, Y.H., 2012. Validation of SMOS brightness temperatures during the HOBE airborne campaign, western Denmark. IEEE Trans. Geosci. Remote Sens. 50, 1468–1482.

Brocca, L., Hasenauer, S., Lacava, T., Melone, F., Moramarco, T., Wagner, W., Dorigo, W., Matgen, P., Martínez-Fernández, J., Llorens, P., Latron, J., Martin, C., Bittelli, M., 2011. Soil moisture estimation through ASCAT and AMSR-E sensors: an inter-comparison and validation study across Europe. Remote Sens. Environ. 115, 3390–3408.

Chan, S., Bindlish, Rajat, O'Neill, Peggy, Njoku, Eni, Jackson, Tom, Colliander, Andreas, Chen, Fan, Burgin, Mariko, Dunbar, Scott, Piepmeier, Jeffrey, Yueh, Simon, Entekhabi, Dara, Cosh, Michael H., Caldwell, Todd, Walker, Jeffrey, Wu, Xiaoling, Berg, Aaron, Rowlandson, Tracy, Pacheco, Anna, McNairn, Heather, Thibeault, Marc, Martínez-Fernández, José, González-Zamora, Ángel, Seyfried, Mark, Bosch, David, Starks, Patrick, Goodrich, David, Prueger, John, Palecki, Michael, Small, Eric E., Zreda, Marek, Calvet, Jean-Christophe, Crow, Wade T., Kerr, Y., 2016. Assessment of the SMAP passive soil moisture product. IEEE Trans. Geosci. Remote Sens. 54, 4994–5007.

Chen, T., McVicar, R.T., Wang, G., Chen, X., de Jeu, A.R., Liu, Y.Y., Shen, H., Zhang, F., Dolman, J.A., 2016. Advantages of using microwave satellite soil moisture over gridded precipitation products and land surface model output in assessing regional vegetation water availability and growth dynamics for a lateral inflow receiving landscape. Remote Sens. 8.

Chen, F., Crow, W.T., Colliander, A., Cosh, M.H., Jackson, T.J., Bindlish, R., Reichle, R.H., Chan, S.K., Bosch, D.D., Starks, P.J., Goodrich, D.C., Seyfried, M.S., 2017a. Application of triple collocation in ground-based validation of soil moisture active/passive (SMAP) level 2 data products. IEEE J. Sel. Top. Appl. Earth Obs. Remote Sens. 10, 489–502.

Chen, Y., Yang, K., Qin, J., Cui, Q., Lu, H., La, Z., Han, M., Tang, W., 2017b. Evaluation of SMAP, SMOS, and AMSR2 soil moisture retrievals against observations from two networks on the Tibetan Plateau. J. Geophys. Res.-Atmos. 122, 5780–5792.

Colliander, A., Jackson, T.J., Bindlish, R., Chan, S., Das, N., Kim, S.B., Cosh, M.H., Dunbar, R.S., Dang, L., Pashaian, L., Asanuma, J., Aida, K., Berg, A., Rowlandson, T., Bosch, D., Caldwell, T., Caylor, K., Goodrich, D., al Jassar, H., Lopez-Baeza, E., Martínez-Fernández, J., González-Zamora, A., Livingston, S., McNairn, H., Pacheco, A., Moghaddam, M., Montzka, C., Notarnicola, C., Niedrist, G., Pellarin, T., Prueger, J., Pulliainen, J., Rautiainen, K., Ramos, J., Seyfried, M., Starks, P., Su, Z., Zeng, Y., van der Velde, R., Thibeault, M., Dorigo, W., Vreugdenhil, M., Walker, J.P., Wu, X., Monerris, A., O'Neill, P.E., Entekhabi, D., Njoku, E.G., Yueh, S., 2017. Validation of SMAP surface soil moisture products with core validation sites. Remote Sens. Environ. 191, 215–231.

Crow, W.T., Berg, A.A., Cosh, M.H., Loew, A., Mohanty, B.P., Panciera, R., Rosnay, P., Ryu, D., Walker, J.P., 2012. Upscaling sparse ground-based soil moisture observations for the validation of coarse-resolution satellite soil moisture products. Rev. Geophys. 50.

Derksen, C., Xu, X., Scott Dunbar, R., Colliander, A., Kim, Y., Kimball, J.S., Black, T.A., Euskirchen, E., Langlois, A., Loranty, M.M., Marsh, P., Rautiainen, K., Roy, A., Royer, A., Stephens, J., 2017. Retrieving landscape freeze/thaw state from Soil Moisture Active Passive (SMAP) radar and radiometer measurements. Remote Sens. Environ. 194, 48–62.

Dorigo, W.A., Wagner, W., Hohensinn, R., Hahn, S., Paulik, C., Xaver, A., Gruber, A., Drusch, M., Mecklenburg, S., van Oevelen, P., Robock, A., Jackson, T., 2011. The International Soil Moisture Network: a data hosting facility for global in situ soil moisture measurements. Hydrol. Earth Syst. Sci. 15, 1675–1698.

Dorigo, W., de Jeu, R., Chung, D., Parinussa, R., Liu, Y., Wagner, W., Fernández-Prieto, D., 2012. Evaluating global trends (1988–2010) in harmonized multi-satellite surface soil moisture. Geophys. Res. Lett. 39, L18405.

Dorigo, W.A., Xaver, A., Vreugdenhil, M., Gruber, A., Hegyiová, A., Sanchis-Dufau, A.D., Zamojski, D., Cordes, C., Wagner, W., Drusch, M., 2013. Global automated quality control of in situ soil moisture data from the international soil moisture network. Vadose Zone J. 12.

Dorigo, W.A., Gruber, A., De Jeu, R.A.M., Wagner, W., Stacke, T., Loew, A., Albergel, C., Brocca, L., Chung, D., Parinussa, R.M., Kidd, R., 2015. Evaluation of the ESA CCI soil moisture product using ground-based observations. Remote Sens. Environ. 162, 380–395.

Dorigo, W., Wagner, W., Albergel, C., Albrecht, F., Balsamo, G., Brocca, L., Chung, D., Ertl, M., Forkel, M., Gruber, A., Haas, E., Hamer, P.D., Hirschi, M., Ikonen, J., de Jeu, R., Kidd, R., Lahoz, W., Liu, Y.Y., Miralles, D., Mistelbauer, T., Nicolai-Shaw, N., Parinussa, R., Pratola, C., Reimer, C., van der Schalie, R., Seneviratne, S.I., Smolander, T., Lecomte, P., 2017. ESA CCI Soil Moisture for improved Earth system understanding: State-of-the art and future directions. Remote Sens. Environ. 203, 185–215.

Draper, C.S., Walker, J.P., Steinle, P.J., de Jeu, R.A.M., Holmes, T.R.H., 2009. An evaluation of AMSR–E derived soil moisture over Australia. Remote Sens. Environ. 113, 703–710.

El Hajj, M., Baghdadi, N., Zribi, M., Rodríguez-Fernández, N., Wigneron, J.P., Al-Yaari, A., Al Bitar, A., Albergel, C., Calvet, J.-C., 2018. Evaluation of SMOS, SMAP, ASCAT and Sentinel-1 soil moisture products at sites in Southwestern France. Remote Sens. 10, 569.

Entekhabi, D., Njoku, E.G., O'Neill, P.E., Kellogg, K.H., Crow, W.T., Edelstein, W.N., Entin, J.K., Goodman, S.D., Jackson, T.J., Johnson, J., Kimball, J., Piepmeier, J.R., Koster, R.D., Martin, N., McDonald, K.C., Moghaddam, M., Moran, S., Reichle, R., Shi, J.C., Spencer, M.W., Thurman, S.W., Leung, T., Van Zyl, J., 2010. The Soil Moisture Active Passive (SMAP) mission. Proc. IEEE 98, 704–716.

Escorihuela, M.J., Chanzy, A., Wigneron, J.P., Kerr, Y.H., 2010. Effective soil moisture sampling depth of L-band radiometry: a case study. Remote Sens. Environ. 114, 995–1001.

Famiglietti, J.S., Ryu, D., Berg, A.A., Rodell, M., Jackson, T.J., 2008. Field observations of soil moisture variability across scales. Water Resour. Res. 44.

FAO, IIASA, ISRIC, ISS-CAS, JRC, 2012. Harmonized World Soil Database (version 1.2). FAO and IIASA, Feb 2012. URL. http://webarchive.iiasa.ac.at/Research/LUC/External-World-soil-database/HWSD_Documentation.pdf, Accessed date: 20 November 2018.

Fernandez-Moran, R., Wigneron, J.P., De Lannoy, G., Lopez-Baeza, E., Parrens, M., Mialon, A., Mahmoodi, A., Al-Yaari, A., Bircher, S., Al Bitar, A., Richaume, P., Kerr, Y., 2017a. A new calibration of the effective scattering albedo and soil roughness parameters in the SMOS SM retrieval algorithm. Int. J. Appl. Earth Obs. Geoinf. 62, 27–38.

Fernandez-Moran, R., Al-Yaari, A., Mialon, A., Mahmoodi, A., Al Bitar, A., De Lannoy, G., Rodriguez-Fernandez, N., Lopez-Baeza, E., Kerr, Y., Wigneron, J.-P., 2017b. SMOS-IC: an alternative SMOS soil moisture and vegetation optical depth product. Remote Sens. 9.

Friedl, M.A., Sulla-Menashe, D., Tan, B., Schneider, A., Ramankutty, N., Sibley, A., Huang, X., 2010. MODIS collection 5 global land cover: algorithm refinements and characterization of new datasets. Remote Sens. Environ. 114, 168–182.

Gruber, A., Dorigo, W.A., Crow, W., Wagner, W., 2017. Triple collocation-based merging of satellite soil moisture retrievals. IEEE Trans. Geosci. Remote Sens. 55, 6780–6792.

Gruber, A., Albergel, Clement, Barrett, Brian, Brocca, Luca, Colliander, Andreas, Cosh, Michael, Crow, Wade, de Jeu, Richard, Dorigo, Wouter, Alemohammad, Seyed Hamed, Martin Hirschi, A.K., Lahoz, William, Loew, Alexander, McColl, Kaighin, Nicolai-Shaw, Nadine, Parinussa, Robert, Pratola, Chiara, Seneviratne, Sonia, Su, Chun-Hsu, van der Schalie, Robin, Wagner, Wolfgang, Zwieback, S., 2019. Validation practices for satellite soil 985 moisture products - What are (the) errors? Remote Sens. Environ (in preparation).

Holgate, C.M., De Jeu, R.A.M., van Dijk, A.I.J.M., Liu, Y.Y., Renzullo, L.J., Vinodkumar, Dharssi, I., Parinussa, R.M., Van Der Schalie, R., Gevaert, A., Walker, J., McJannet, D., Cleverly, J., Haverd, V., Trudinger, C.M., Briggs, P.R., 2016. Comparison of remotely sensed and modelled soil moisture data sets across Australia. Remote Sens. Environ. 186, 479–500.

Jackson, T.J., Schmugge, T.J., Wang, J.R., 1982. Passive microwave sensing of soil moisture under vegetation canopies. Water Resour. Res. 18, 1137–1142.

Jackson, T.J., Bindlish, R., Cosh, M.H., Tianjie, Z., Starks, P.J., Bosch, D.D., Seyfried, M., Moran, M.S., Goodrich, D.C., Kerr, Y.H., Leroux, D., 2012. Validation of soil moisture and ocean salinity (SMOS) soil moisture over watershed networks in the U.S. IEEE Trans. Geosci. Remote Sens. 50, 1530–1543.

Jacquette, E., Al Bitar, A., Cabot, F., Mialon, A., Richaume, P., Quesney, A., Berthon, L., 2013. CATDS SMOS L3 soil moisture retrieval processor Algorithm Theoretical Baseline Document (ATBD). available at. http://www.cesbio.ups-tlse.fr/SMOS_blog/wp-content/uploads/2013/08/ATBD_L3_rev2_draft.pdf, Accessed date: 4 January 2015.

Jones, L.A., Kimball, J.S., Reichle, R.H., Madani, N., Glassy, J., Ardizzone, J.V., Colliander, A., Cleverly, J., Desai, A.R., Eamus, D., Euskirchen, E.S., Hutley, L., Macfarlane, C., Scott, R.L., 2017. The SMAP level 4 carbon product for monitoring ecosystem land–atmosphere CO_2 exchange. IEEE Trans. Geosci. Remote Sens. 55, 6517–6532.

Jung, M., Reichstein, M., Schwalm, C.R., Huntingford, C., Sitch, S., Ahlström, A., Arneth, A., Camps-Valls, G., Ciais, P., Friedlingstein, P., Gans, F., Ichii, K., Jain, A.K., Kato, E., Papale, D., Poulter, B., Raduly, B., Rödenbeck, C., Tramontana, G., Viovy, N., Wang, Y.-P., Weber, U., Zaehle, S., Zeng, N., 2017. Compensatory water effects link yearly global land CO_2 sink changes to temperature. Nature 541, 516.

Kerr, Y.H., Waldteufel, P., Wigneron, J.P., Martinuzzi, J., Font, J., Berger, M., 2001. Soil moisture retrieval from space: the Soil Moisture and Ocean Salinity (SMOS) mission. IEEE Trans. Geosci. Remote Sens. 39, 1729–1735.

Kerr, Y.H., Waldteufel, P., Wigneron, J.P., Delwart, S., Cabot, F., Boutin, J., Escorihuela, M.J., Font, J., Reul, N., Gruhier, C., Juglea, S.E., Drinkwater, M.R., Hahne, A., Martin-Neira, M., Mecklenburg, S., 2010. The SMOS mission: new tool for monitoring key elements ofthe global water cycle. Proc. IEEE 98, 666–687.

Kerr, Y.H., Waldteufel, P., Richaume, P., Wigneron, J.P., Ferrazzoli, P., Mahmoodi, A., Al Bitar, A., Cabot, F., Gruhier, C., Juglea, S.E., Leroux, D., Mialon, A., Delwart, S., 2012. The SMOS soil moisture retrieval algorithm. IEEE Trans. Geosci. Remote Sens. 50, 1384–1403.

Kerr, Y.H., Al-Yaari, A., Rodriguez-Fernandez, N., Parrens, M., Molero, B., Leroux, D., Bircher, S., Mahmoodi, A., Mialon, A., Richaume, P., Delwart, S., Al Bitar, A., Pellarin, T., Bindlish, R., Jackson, T.J., Rüdiger, C., Waldteufel, P., Mecklenburg, S., Wigneron, J.P., 2016. Overview of SMOS performance in terms of global soil moisture monitoring after six years in operation. Remote Sens. Environ. 180, 40–63.

Kolassa, J., Reichle, R.H., Liu, Q., Alemohammad, S.H., Gentine, P., Aida, K., Asanuma, J., Bircher, S., Caldwell, T., Colliander, A., Cosh, M., Holifield Collins, C., Jackson, T.J., Martínez-Fernández, J., McNairn, H., Pacheco, A., Thibeault, M., Walker, J.P., 2018. Estimating surface soil moisture from SMAP observations using a Neural Network technique. Remote Sens. Environ. 204, 43–59.

Koster, R.D., Dirmeyer, P.A., Guo, Z., Bonan, G., Chan, E., Cox, P., Gordon, C.T., Kanae, S., Kowalczyk, E., Lawrence, D., Liu, P., Lu, C.-H., Malyshev, S., McAvaney, B., Mitchell, K., Mocko, D., Oki, T., Oleson, K., Pitman, A., Sud, Y.C., Taylor, C.M., Verseghy, D., Vasic, R., Xue, Y., Yamada, T., 2004. Regions of strong coupling between soil moisture and precipitation. Science 305, 1138–1140.

Kottek, M., Grieser, J., Beck, C., Rudolf, B., Rubel, F., 2006. World Map of the Köppen-Geiger climate classification updated. Meteorol. Z. 15, 259–263.

Liu, Y.Y., Dorigo, W.A., Parinussa, R.M., de Jeu, R.A.M., Wagner, W., McCabe, M.F., Evans, J.P., van Dijk, A.I.J.M., 2012. Trend-preserving blending of passive and active microwave soil moisture retrievals. Remote Sens. Environ. 123, 280–297.

Masson, V., Champeaux, J.-L., Chauvin, F., Meriguet, C., Lacaze, R., 2003. A global database of land surface parameters at 1-km resolution in meteorological and climate models. J. Clim. 16, 1261–1282.

Miralles, D.G., van den Berg, M.J., Gash, J.H., Parinussa, R.M., de Jeu, R.A.M., Beck, H.E., Holmes, T.R.H., Jiménez, C., Verhoest, N.E.C., Dorigo, W.A., Teuling, A.J., Johannes Dolman, A., 2014a. El Niño–La Niña cycle and recent trends in continental evaporation. Nat. Clim. Chang. 4, 122–126.

Miralles, D.G., Teuling, A.J., van Heerwaarden, C.C., Vila-Guerau de Arellano, J., 2014b. Mega-heatwave temperatures due to combined soil desiccation and atmospheric heat accumulation. Nat. Geosci. 7, 345–349.

Mo, T., Choudhury, B.J., Schmugge, T.J., Wang, J.R., Jackson, T.J., 1982. A model for microwave emission from vegetation-covered fields. J. Geophys. Res. Oceans 87, 11229–11237.

Oliva, R., Daganzo, E., Richaume, P., Kerr, Y., Cabot, F., Soldo, Y., Anterrieu, E., Reul, N., Gutierrez, A., Barbosa, J., Lopes, G., 2016. Status of Radio Frequency Interference (RFI) in the 1400–1427 MHz passive band based on six years of SMOS mission. Remote Sens. Environ. 180, 64–75.

O'Neill, P., Chan, S., Bindlish, R., Jackson, T., Colliander, A., Dunbar, S., Chen, F., Piepmeier, J., Yueh, S., Entekhabi, D., Cosh, M., Caldwell, T., Walker, J., Wu, X., Berg, A., Rowlandson, T., Pacheco, A., McNairn, H., Thibeault, M., Martínez-Fernández, J., González-Zamora, Á., Lopez-Baeza, E., Udall, F., Seyfried, M., Bosch, D., Starks, P., Holifield, C., Prueger, J., Su, Z., Velde, R.v.d., Asanuma, J., Palecki, M., Small, E., Zreda, M., Calvet, J.C., Crow, W., Kerr, Y., 2017. Assessment of version 4 of the SMAP passive soil moisture standard product. In: 2017 IEEE International Geoscience and Remote Sensing Symposium (IGARSS), pp. 3941–3944.

Parrens, M., Zakharova, E., Lafont, S., Calvet, J.C., Kerr, Y., Wagner, W., Wigneron, J.P., 2012. Comparing soil moisture retrievals from SMOS and ASCAT over France. Hydrol. Earth Syst. Sci. 16, 423–440.

Parrens, M., Wigneron, J.-P., Richaume, P., Mialon, A., Al Bitar, A., Fernandez-Moran, R., Al-Yaari, A., Kerr, Y.H., 2016. Global-scale surface roughness effects at L-band as estimated from SMOS observations. Remote Sens. Environ. 181, 122–136.

Paulik, C., Dorigo, W., Wagner, W., Kidd, R., 2014. Validation of the ASCAT Soil Water Index using in situ data from the International Soil Moisture Network. Int. J. Appl. Earth Obs. Geoinf. 30, 1–8.

Pierdicca, N., Luca, P., Fabio, F., Raffaele, C., Marco, T., 2013. Analysis of two years of ASCAT- and SMOS-derived soil moisture estimates over Europe and North Africa. Eur. J. Remote Sens. 46, 759–773.

Pitman, A.J., 2003. The evolution of, and revolution in, land surface schemes designed for climate models. Int. J. Climatol. 23, 479–510.

PUM, 2016. Product User Manual (PUM) Soil Moisture Data Records, Metop ASCAT Soil Moisture Time Series. Doc. No: SAF/HSAF/CDOP2/PUM, v0.4, 2016. http://hsaf.meteoam.it/documents/PUM/SSM_ASCAT_DR_PUM_v0.4.pdf.

Reichle, R.H., De Lannoy, G.J.M., Liu, Q., Ardizzone, J.V., Colliander, A., Conaty, A., Crow, W., Jackson, T.J., Jones, L.A., Kimball, J.S., Koster, R.D., Mahanama, S.P., Smith, E.B., Berg, A., Bircher, S., Bosch, D., Caldwell, T.G., Cosh, M., González-Zamora, Á., Holifield Collins, C.D., Jensen, K.H., Livingston, S., Lopez-Baeza, E., Martínez-Fernández, J., McNairn, H., Moghaddam, M., Pacheco, A., Pellarin, T., Prueger, J., Rowlandson, T., Seyfried, M., Starks, P., Su, Z., Thibeault, M., van der Velde, R., Walker, J., Wu, X., Zeng, Y., 2017. Assessment of the SMAP level-4 surface and root-zone soil moisture product using in situ measurements. J. Hydrometeorol. 18, 2621–2645.

Rodell, M., Houser, P.R., Jambor, U., Gottschalck, J., Mitchell, K., Meng, C.J., Arsenault, K., Cosgrove, B., Radakovich, J., Bosilovich, M., Entin, J.K., Walker, J.P., Lohmann, D., Toll, D., 2004. The global land data assimilation system. Bull. Am. Meteorol. Soc. 85, 381–394.

Rodríguez-Fernández, J.N., Kerr, H.Y., van der Schalie, R., Al-Yaari, A., Wigneron, J.-P., de Jeu, R., Richaume, P., Dutra, E., Mialon, A., Drusch, M., 2016. Long term global surface soil moisture fields using an SMOS-trained neural network applied to AMSR-E data. Remote Sens. 8.

Rubel, F., Brugger, K., Haslinger, K., Auer, I., 2017. The climate of the European Alps: shift of very high resolution Köppen-Geiger climate zones 1800–2100. Meteorol. Z. 26, 115–125.

Sahoo, A.K., Houser, P.R., Ferguson, C., Wood, E.F., Dirmeyer, P.A., Kafatos, M., 2008. Evaluation of AMSR-E soil moisture results using the in-situ data over the Little River Experimental Watershed, Georgia. Remote Sens. Environ. 112, 3142–3152.

Saxton, K.E., Rawls, W.J., 2006. Soil water characteristic estimates by texture and organic matter for hydrologic solutions. Soil Sci. Soc. Am. J. 70, 1569–1578.

Seneviratne, S.I., Corti, T., Davin, E.L., Hirschi, M., Jaeger, E.B., Lehner, I., Orlowsky, B., Teuling, A.J., 2010. Investigating soil moisture–climate interactions in a changing climate: a review. Earth Sci. Rev. 99, 125–161.

Seneviratne, S.I., Wilhelm, M., Stanelle, T., van den Hurk, B., Hagemann, S., Berg, A., Cheruy, F., Higgins, M.E., Meier, A., Brovkin, V., Claussen, M., Ducharne, A., Dufresne, J.-L., Findell, K.L., Ghattas, J., Lawrence, D.M., Malyshev, S., Rummukainen, M., Smith, B., 2013. Impact of soil moisture-climate feedbacks on CMIP5 projections: first results from the GLACE-CMIP5 experiment. Geophys. Res. Lett. 40, 5212–5217.

Su, C.-H., Ryu, D., Young, R.I., Western, A.W., Wagner, W., 2013. Inter-comparison of microwave satellite soil moisture retrievals over the Murrumbidgee Basin, southeast Australia. Remote Sens. Environ. 134, 1–11.

Wagner, W., Lemoine, G., Rott, H., 1999. A method for estimating soil moisture from ERS scatterometer and soil data. Remote Sens. Environ. 70, 191–207.

Wagner, W., Hahn, S., Kidd, R., Melzer, T., Bartalis, Z., Hasenauer, S., Figa-Saldaña, J., de Rosnay, P., Jann, A., Schneider, S., Komma, J., Kubu, G., Brugger, K., Aubrecht, C., Züger, J., Gangkofner, U., Kienberger, S., Brocca, L., Wang, Y., Blöschl, G., Eitzinger, J., Steinnocher, K., 2013. The ASCAT soil moisture product: a review of its specifications, validation results, and emerging applications. Meteorol. Z. 22, 5–33.

Wigneron, J.P., Waldteufel, P., Chanzy, A., Calvet, J.C., Kerr, Y., 2000. Two-dimensional microwave interferometer retrieval capabilities over land surfaces (SMOS mission). Remote Sens. Environ. 73, 270–282.

Wigneron, J.P., Kerr, Y., Waldteufel, P., Saleh, K., Escorihuela, M.J., Richaume, P., Ferrazzoli, P., de Rosnay, P., Gurney, R., Calvet, J.C., Grant, J.P., Guglielmetti, M., Hornbuckle, B., Mätzler, C., Pellarin, T., Schwank, M., 2007. L-band Microwave Emission of the Biosphere (L-MEB) Model: description and calibration against experimental data sets over crop fields. Remote Sens. Environ. 107, 639–655.

Wigneron, J.P., Jackson, T.J., O'Neill, P., De Lannoy, G., de Rosnay, P., Walker, J.P., Ferrazzoli, P., Mironov, V., Bircher, S., Grant, J.P., Kurum, M., Schwank, M., Munoz-Sabater, J., Das, N., Royer, A., Al-Yaari, A., Al Bitar, A., Fernandez-Moran, R., Lawrence, H., Mialon, A., Parrens, M., Richaume, P., Delwart, S., Kerr, Y., 2017. Modelling the passive microwave signature from land surfaces: a review of recent results and application to the L-band SMOS & SMAP soil moisture retrieval algorithms. Remote Sens. Environ. 192, 238–262.